Beams-doc-xxxx

Proposal for Experiments and Upgrades at the A0 Photoinjector

Editor: Mike Church

Contributors: Leo Bellantoni, Nathan Eddy, Don Edwards, Helen Edwards, Ralph Fiorito, Ray Fliller, Elvin Harms, Grigory Kazakevich, Tim Koeth, Alex Lumpkin, Sergei Nagaitsev, Philippe Piot, Jinhao Ruan, Vic Scarpine, Bill Soyars, Yin-e Sun, Mike Syphers, Randy Thurman-Keup, Manfred Wendt

August 11, 2008

Table of Contents

1 Introduction

The Fermilab A0 photoinjector is a 16 MeV electron linac located in the A0 service building above the Tevatron beam enclosure. Since 1992 it has been used for accelerator research and training in the development and operation of electron injectors, lasers, and superconducting RF systems [1]. The photoinjector consists of a 1.3 GHz normal conducting RF gun with a Cs_2Te photocathode, a low gradient 1.3GHz TESLA technology "capture" cavity, a transport channel for experiments and diagnostics, a 45° bend to a dump, and a user experimental area. The beam parameters and the current beamline layout are shown in Appendices 7.1 and 7.2, respectively.

The injector can be configured to provide both compressed and uncompressed beam. The bunch structure of the beam is similar to the TESLA Test Facility at DESY, with 1 μs bunch spacing and bunch trains up to 200 μs duration. Bunch charge up to 10 nC has been available, and such high charge bunches have been used in successful plasma wakefield experiments [2].

Another area of focus has been round-to-flat beam transformation experiments in which equal emittances in the two transverse planes are repartitioned to give a very large relative ratio of 100:1. This experiment required the addition of a three quadrupole "transformer" and the ability to provide magnetic field (B_z) on the cathode. It was completed in 2005 [3]. Other experiments at this time included the characterization of the bunch compression with two macroparticles [4].

The present ongoing experiment attempts to perform efficient emittance exchange between the longitudinal plane and one transverse plane. This experiment has required a reconfiguration of the beam line. The magnetic chicane was removed and reconfigured into a two dogleg arrangement with a deflecting mode cavity after the first dogleg. The deflecting mode cavity was previously developed in a superconducting version for an HEP experiment [5]. The emittance exchange experiment, with its very short bunch lengths, has reemphasized the need for developing better methods of bunch length measurement. Present experiments typically use 1 nC bunch charge, and at this intensity coherent synchrotron radiation (CSR) can be important. In order to enable the study of CSR, we are proposing the reinstallation of a magnetic chicane in addition to the double dogleg configuration.

This proposal addresses the following experimental themes.

<u>Theme 1: Generation, transport, and manipulation of high-brightness electron beams</u>

The next generation of the emittance exchange experiment will focus on emittance measurements after the exchange for different initial transverse and longitudinal phase space configurations and bunch charges. The focus will include investigations into CSR effects, which we expect are present. These effects, and their mitigation, need to be understand before a design for the NML injector is finalized. We will also investigate the possibility of bunch train generation at the sub ps level from single bunches. We expect strong collaboration with ANL and NIU on these experiments.

The longer term theme of emittance manipulation includes the improvement of the round-to-flat beam transformation and it adaptation toward other uses such as the image charge undulator. We will also be considering the possibilities with coupling flat and longitudinal manipulations. These manipulations are a key part of a number of ideas such as polarized RF gun development which,

when coupled together, could evolve into the generation of an ILC-like beam to inject into the linac without the need of a damping ring.

Transverse adiabatic capture of a ring beam is an accelerator physics concept that has been developed by Y. Derbenev [6] and requires a proof-of-principle experiment. This concept incorporates the flat beam transformation and possibly the emittance exchange. It might help in the goal of developing ILC-like injector parameters. We plan to study how it could be implemented but don't expect to be able to complete this experiment until the photoinjector is moved to NML.

Microbunching of high intensity compressed beams from (presumably) a combination of CSR and space charge effects has recently been identified as a source of error in emittance diagnostics of such beams. We propose a series of experiments to study this effect to further understand it and to possibly mitigate it [7].

Theme 2: Electromagnetic radiation generation using non-ultra-relativistic electron beams

An image charge undulator (Smith-Purcell radiation from two parallel gratings) has not yet been experimentally demonstrated, and we propose to build a proof-of-principal experiment. This experiment will be carried out with a flat beam. Once we complete the calculations and understand what the experimental configuration will be, we will build and carry out a first generation of the experiment and compare with expectations. We expect strong collaboration with ANL and NIU.

We are considering the possibility of developing an experiment to generate x-rays from inverse Compton scattering for the purpose of characterizing the dependence of the x-ray spectrum properties on the electron beam parameters. This experiment will require collaboration with a group with strong laser expertise and interest in developing intense laser sources. A compact high peak bunch energy laser will be a step toward generation of intense x-rays with modest accelerators. A lower bunch energy laser will be sufficient to characterize the optimization of the parameter space.

Theme 3: Diagnostic experiments

There are a number of beam diagnostic instruments that we are currently developing and will continue to develop in the near time scale. In particular, we are developing several promising techniques for bunch length monitoring. One technique using coherent transition radiation (CTR) from a flat screen radiator, one technique using Martin-Puplett interferometry, and one non-intercepting technique using electro-optical (EO) sampling.

Theme 4: Technology development

All of the above proposed experiments will benefit from better bunch length diagnostics To this end we are proposing the addition of a 3.9 GHz deflecting mode cavity. The cavity will be able to benchmark a number of other diagnostics under development. A new deflecting mode cavity will also allow us to improve on the design for the suppression of unwanted cavity modes excited by the beam.

The A0 photoinjector group is also interested in developing a spin polarized RF gun using a GaAs photocathode. This photocathode is extremely sensitive to vacuum conditions in the gun, and to date has only been successfully used in DC guns. Fermilab is collaborating with DULY Research Inc. to produce a Plane Wave Transformer (PWT) gun which has an open RF structure

which will allow for greater pumping via a sputtered non-evaporate getter (SNEG) coating. To this end, A0 has a cathode preparation chamber for GaAs photocathodes which has yet to be commissioned. DULY Research Inc is building the gun, and is funded by a Phase II SBIR.

Another technology that may prove useful for a spin polarized electron RF gun is a superconducting RF gun. Such a gun will have excellent vacuum and may support such a cathode. BNL is already pursuing this course, and we hope to leverage our SRF infrastructure to collaborate with them on this project.

LLRF development is a core development for many plans at FNAL. The A0 Photoinjector with its different cavity systems and beam is an ideal and unique test bed at FNAL for this development.

In addition to near term work on the cathode drive laser and the development of a laser for an EO system, we have plans to become knowledgeable in fiber laser technology as this technology may provide better and less costly alternatives to today's solutions.

It is worth noting that with a higher energy beam the laser acceleration experiment proposed by Melissinos [8][9] using a ring structure laser would be possible. We are not at this time considering this experiment. Also with our large bunch charge capability (~10 nC), plasma experiments are possible and have been done at A0 in the past. We do not plan to pursue these experiments at present as very competitive work is being done elsewhere.

References

[1] *Fermilab NICADD Photoinjector Laboratory*, WWW Document, (http://nicadd.niu.edu/fnpl/).

[2] N. Barov *et al.*, Phys. Rev. ST Accel. Beams **7**, 061301 (2004).

[3] P. Piot *et al.*, Phys. Rev. ST Accel. Beams **9**, 031001 (2006).

[4] R. Tikhoplav *et al.*, "Investigation of the Longitudinal Beam Dynamics in a Photoinjector Using a Two-macroparticle Model", in *Proc. LINAC2004, Lubeck, Germany*.

[5] C. Adolphsen *et al.*, EuroTev Report 2007-10 (2007).

[6] Y. Derbenev, NIM A **441**, 223 (2000).

[7] A.H. Lumpkin, *et al*., "Observation of Enhanced OTR Signals from a Compressed Electron Beam", in *Proc. BIW2008, Lake Tahoe, CA* (to be published).

[8] R. Tikhoplav *et al.*, in *Proc. of EPAC2002, Paris, France*, p. 984.

[9] P. Piot, A. Melissinos, R. Tikhoplav, in *Proc. of PAC2005, Knoxville, TN*, p. 2503.

2 Beam physics experiments

2.1 Emittance exchange experiments and CSR studies

Transverse to longitudinal emittance exchange was proposed by Y. Orlov et al. in 1991 [1]. In 2006, Cornacchia and Emma proposed an approximate exchange which consists of a dipole mode cavity flanked by two doglegs of opposite sign [2]. Kim modified the optics to achieve exact emittance exchange [3]. Based on Kim's optics, a transverse to longitudinal emittance exchange experiment is currently being performed at A0. The goals of the experiment are: demonstrate proof-of-principle, study the dynamics of the exchange, understand emittance diluting effects in the exchange, and develop mitigating strategies for the dilution. This experiment uses two doglegs with a deflecting mode cavity between them to exchange the horizontal and longitudinal emittances. This is followed by a short diagnostics section and a vertical spectrometer before the beam dump.

For a perfect emittance exchange the 4x4 transverse/longitudinal transport matrix is of the form

$$R = \begin{pmatrix} A_{11} & A_{12} & B_{11} & B_{12} \\ A_{21} & A_{22} & B_{21} & B_{22} \\ C_{11} & C_{12} & D_{11} & D_{12} \\ C_{21} & C_{22} & D_{21} & D_{22} \end{pmatrix}.$$

Following the notation of D. Edwards [4], let α be the bend of each magnet in a dogleg and L_1 the distance between bends, then the dog leg matrix is given by

$$M_{dog} = \begin{pmatrix} 1 & L_1 & 0 & \alpha L_1 \\ 0 & 1 & 0 & 0 \\ 0 & \alpha L_1 & 1 & \alpha^2 L_1 \\ 0 & 0 & 0 & 1 \end{pmatrix} = \begin{pmatrix} 1 & D/\alpha & 0 & D \\ 0 & 1 & 0 & 0 \\ 0 & D & 1 & \alpha D \\ 0 & 0 & 0 & 1 \end{pmatrix}$$

where D is the dispersion. Let this be followed by a drift, L_2 to a thin lens deflection mode cavity. The cavity matrix is given by

$$M_{cav} = \begin{pmatrix} 1 & 0 & 0 & 0 \\ 0 & 1 & T & 0 \\ 0 & 0 & 1 & 0 \\ T & 0 & 0 & 1 \end{pmatrix}.$$

Where for exchange T= -1/D $= \dfrac{-1}{\alpha L_1} = \dfrac{\omega}{c}\dfrac{eV_{cav}}{E_{beam}}$ and V_{cav} is the deflection strength of the cavity and E_{beam} is the beam energy.

The total exchange is

$$M_{dog}L_2M_{cav}L_2M_{dog} = \begin{pmatrix} 0 & 0 & -\frac{1}{\alpha}-\frac{L_2}{D} & -L_2\alpha \\ 0 & 0 & \frac{-1}{D} & -\alpha \\ -\alpha & -\alpha L_2 & 0 & 0 \\ \frac{-1}{D} & \frac{-1}{\alpha}-\frac{L_2}{D} & 0 & 0 \end{pmatrix}.$$

In our geometry D=0.33 m and $\alpha = 22.5°$.

For a finite length cavity, the (4,3) element of M_{cav} enters and the on-diagonal (coupling) blocks start to show nonzero values and will dilute the 2D emittances, especially the smaller one. The finite length cavity also causes the equilibrium orbit to follow a staircase trajectory through the cavity. These effects can be compensated to some extent by suitable choices of beam and cavity parameters.

The A0 experiment attempts to exchange a 6 mm-rad normalized transverse emittance with a 120 mm-rad (204 keV-ps) normalized longitudinal emittance. The beamline was commissioned in the summer of 2007 and measurements of the transport matrix are underway. Preliminary data has been taken of the beam emittances before and after the exchange, and analysis of that data is ongoing and will be the Ph.D. thesis of Tim Koeth. The layout of the current beamline is shown in Figure 7.1 in Appendix 7.2.

After initial evidence that the emittance exchange was occurring, our experimental program has concentrated on measuring the 6-D emittance exchange transport matrix. Figure 2.1 shows preliminary results of the transport matrix measurements as a function of cavity strength T. The circles represent the data and the red lines are what is expected from the model. The agreement is quite good for 12 of the 16 elements. We think the discrepancy in the remaining elements is due to errors in the model, in particular how the dipoles are handled.

These measurements have shown a need for improved diagnostics. In particular, we are preparing a Martin-Puplett interferometer for measuring sub-picosecond bunch lengths and larger OTR screens to image the resulting large transverse beam spot. Additionally we have begun to measure the synchrotron and coherent synchrotron radiation that is a consequence of the beam parameters and beamline geometry.

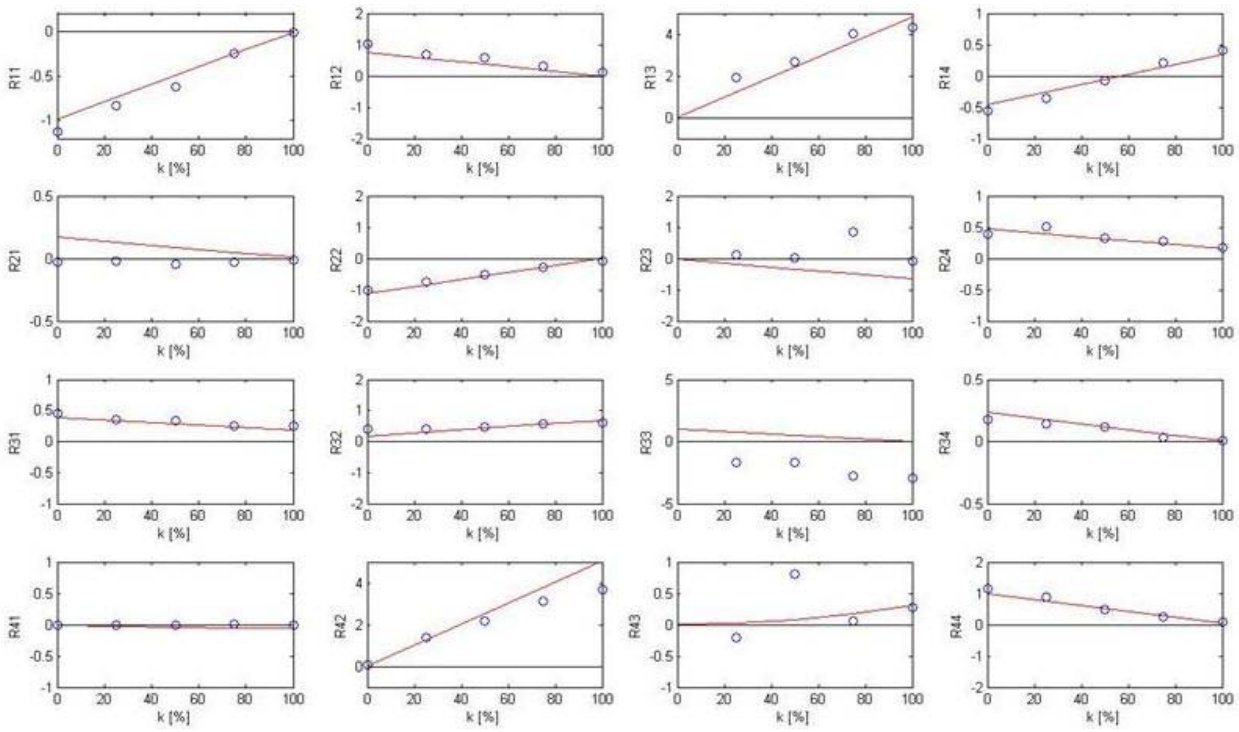

Figure 2.1: The transport matrix as a function of k (= T in the text). The circles are the measurements. The red lines are derived from the ELEGANT model.

We are proposing to continue and expand this experiment with the following program.

Step 1: Measure the emittance exchange

The transverse emittances are measured with a multislit screen which gives a complete picture of the transverse phase space ellipse. The longitudinal emittance measurements are currently limited to separate energy spread and bunch length measurements which provide an upper bound on the longitudinal emittance. Energy spread is measured with a beam screen after a spectrometer, and the bunch length is measured using a streak camera for bunches longer than 1 ps, and Martin-Puplett interferometer for bunches shorter than 1 ps. Currently the instrumentation is not configured to measure the energy-time correlation of the bunch either at the input or the output of the exchanger. However, it may be possible to transport the light from the screen after the spectrometer to the streak camera, which would give us the energy-time correlation.

Step 2: Manipulate the input phase space ellipse to tune the output phase space ellipse

Tuning the input transverse phase space ellipse will modify the output longitudinal phase space ellipse and vice versa. We can tune the beam for short bunches, or low momentum spread, by adjusting the spot size prior to the exchange. Adjusting the input energy chirp of the beam will adjust the output transverse phase space ellipse. The reason to study the effect of the input phase space ellipses is to look for different output conditions like shorter bunches and for the effects of non-zero elements in the A and D blocks of the transport matrix due to the finite length cavity. These elements will lead to coupling of the emittances and increase the measured emittances after the exchange. This effect is most dramatic in the longitudinal emittance after the exchange

since it is the smaller of the two. These measurements will be done at the low charge of 100 pC/bunch to reduce effects of space charge (SC) and CSR. These two effects increase the beam emittance and distort the phase space.

It has been pointed out recently that sub-ps bunch trains can be generated from a single bunch by inserting a slit mask upstream of the exchanger [5]. The beamlets generated in x-space will be converted to a bunch train after the exchange. An additional compressor stage may be necessary to make the beamlets upright in z-dp space.

Step 3: Understand the impact of collective effects in the exchanger

At high charge, CSR and SC can become a major source of emittance dilution. These effects induce energy spread changes in the bunch as it passes through each dipole of the exchanger. Measurements with a pyrodetector located at the spectrometer at A0 show that CSR is present at $\geq$1 nC bunch charge. These measurements show that the radiated power scales as $Q^2/\sigma_z^{4/3}$ and that the beam energy spread and spot size after the straight ahead spectrometer show reasonable agreement with CSRtrack [6] simulations for the case of low energy spread. Measurements also show coherent radiation in the third dipole of the emittance exchange beamline. For these reasons we wish to study the effects of CSR and SC in the emittance exchange experiment.

One step will be to understand the radiation seen from the dipoles. We will measure the radiation power vs. bunch charge and length at all available dipoles. This will tell us in which magnets CSR is being produced and where to place instrumentation. Once we know where to place instrumentation, the next series of experiments will be to determine the exact nature of the emitted radiation. Electrons emit edge radiation when passing through the fringe field of the dipoles, and for short enough bunches this radiation can be coherent. Some of the dipoles have ports that are capable of seeing both types of radiation – edge and body radiation. Body synchrotron radiation is polarized mostly in the plane of the bend. Edge radiation is radially polarized. Measurements with a polarizer done in the plane of each bend can determine the nature of the radiation, assuming the wakefields in the vacuum chamber to not contribute significantly to the radiation field The available Martin-Puplett interferometer can be used to measure the coherence time of the radiation. Not only will this give a bunch length measurement in the dipole, it will verify that the radiation is indeed coherent, as incoherent radiation will not give an interferogram.

CSR and SC beam effects have been studied in bunch compressors in the Pegasus Lab at UCLA, at the ATF at Brookhaven, and FLASH at DESY [7][8][9]. These measurements showed transverse and longitudinal beam breakup as a result of compression. Coherent edge radiation has also led to beam breakup at the ATF bunch compressor [10]. Our program will be able to investigate higher charge beams, in an emittance exchange beamline with beams not represented by one dimensional CSR models.

Measurements of CSR and space charge in the emittance exchange beamline will focus around understanding where in the exchanger the beam is most sensitive to blowup from CSR. The analytical CSR model, e.g. used in ELEGANT, assumes the bunch to be an ultrarelativistic one-dimensional line charge. For the emittance exchange experiment this will not be a valid approximation, therefore studying the CSR is useful for discovering new physics and testing models and numerical simulations. The photoinjector is also the only place that these effects can be understood in the arena of emittance exchange. Because the phase spaces are undergoing the

exchange as the CSR and space charge are acting, it is not clear from the previous studies of bunch compression how this will affect the beam.

In one scenario we will tune the input beam to fully compress the bunch after the exchanger and measure the output emittances and radiation power as the charge is increased. In a second scenario we will compress the bunch at the deflecting cavity and repeat the measurements. These measurements will then indicate if CSR is more dominant in the first or second dogleg. After these measurements, the input beam parameters can be tuned to minimize the effects of CSR in the exchanger at high charge and obtain an emittance that is as small as possible. Since predicting CSR effects in the exchange cannot be done using the 1D models, this will require simulations to show the interesting parameters to start with.

By replacing the deflecting cavity with a quadrupole channel, one can use the double dogleg as a bunch compressor. A dogleg bunch compressor has a negative R_{56}, the opposite sign of a chicane or S type compressor. This means the input bunch needs to be chirped in the opposite fashion for compression. This may change the effects of CSR and SC. The A0 upgrade will also include a chicane type compressor. If these are designed to have the same magnitude R_{56}, then the effects can be compared in each compressor. These experiments can be done at higher charge than the UCLA and BNL experiments, perhaps showing regimes where SC alone is not sufficient to explain the beam behavior.

Step 4: Understand the effects of CSR in the compressor.

It is important to understand the effects of CSR in the bunch compressor for the design of the injector at NML. To that end, each dipole of the bunch compressor will have ports capable of seeing synchrotron radiation. The beam will be measured going through the compressor with a chirp that will compress the bunch, a chirp that will not compress the bunch, and a chirp that will over compress the bunch. Each time the charge, transverse emittance before and after the compressor, bunch length before and after compressor, beam profile after the spectrometer, and radiation power in each dipole will be measured. The same set of data will also be collected for the same bunches not going through the compressor to separate effects of space charge and CSR in the spectrometer magnet. These measurements will give a complete picture of CSR and its effect in the compressor.

Previous simulations from DESY show that the transverse optics in the compressor can have a large effect on the transverse emittance growth after the compressor [9]. In particular, the location of the waist in the bunch compressor has a large effect on the emittance growth. We will measure the emittance growth as a function of the input phase space ellipse and determine the optics to provide a minimum emittance after compression.

Step 5: Arbitrary tailoring of the current distribution of a relativistic electron bunch.

Very recently a scheme to arbitrarily shape the current profile of an electron beam was proposed [11]. The technique relies on the emittance exchanger in the following way. An incoming beam is first transversely shaped upstream of the exchanger; then the emittance exchanger maps the transverse profile into the time profile thereby resulting in a tailored time distribution. Tailoring the longitudinal profile of an electron beam has tremendous applications ranging from super-radiant operation of a free-electron laser (by using a beam consisting of microbunches) to several advanced accelerator concepts: linearly ramped bunches are known to increase the transformer ratio in beam-driven acceleration techniques (such as dielectric and plasma wakefield

acceleration). Preliminary calculations indicate the possibility to, e.g., generate bunch trains with 80 fs spacing at 15 MeV (see Figure 2.2). At A0 the generation of sub-picosecond bunch trains could be directly observed downstream of the emittance exchanger by a suitable choice of slits parameters. The main diagnostics would be a sensitive THz detector to measure the coherent transition radiation produced by such a train of bunches.

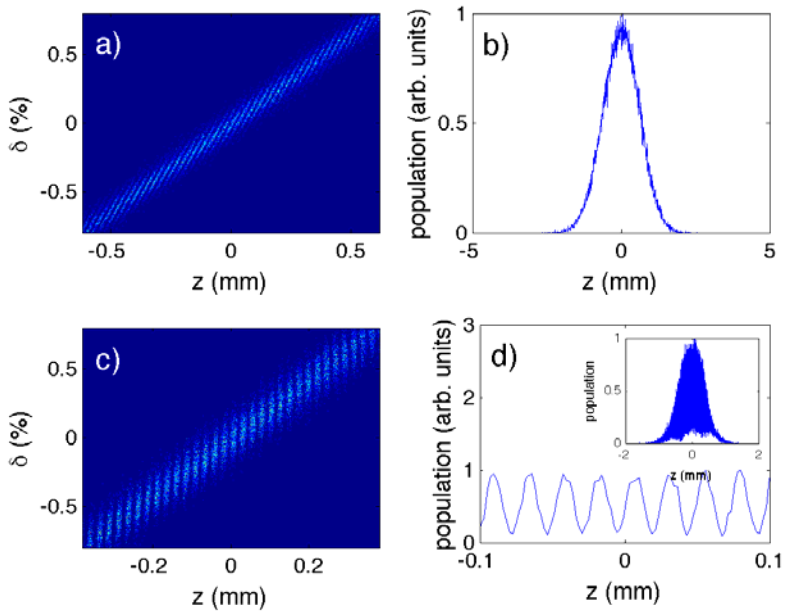

Figure 2.2: Example of pulse train generation using a transverse-to-longitudinal emittance exchanger. Zoomed longitudinal phase space (a) and corresponding longitudinal projection (b) downstream of the exchanger. Zoomed longitudinal phase space (c) and associated projection (d) downstream of a small magnetic chicane (in this case R56=0.03 m). The incoming beam upstream of the exchanger was passed through a series of horizontal slits with 0.1 mm width and 0.2 mm spacing (edge-to-edge). The inset in plot (d) correspond to the profile over the full bunch extent while the main plot is a zoom for $-0.1 < z\ (\text{mm}) < 0.1$.

2.2 Round-to-flat beam transformation and image charge undulator

High intensity x-rays can be generated from large synchrotron radiation or FEL facilities using electrons beams at GeV energies. The image charge undulator (ICU) [12][13] offers an opportunity to generate high intensity x-rays using electron beams of much lower energy generated by a much more compact and less expensive electron source. With sub-millimeter gratings, the radiation produced by an ICU can be in the hard x-ray regime for an electron beam energy less than 200 MeV. Currently, there has not been an experimental demonstration of the image charge undulator. At A0 we have the experience of producing flat electron beams with emittance ratio 100:1 [14] with normalized rms beam emittance of 0.4 and 40 μm. This represents an advantage to pursue a proof-of-principle image charge undulator experiment using planar gratings.

An ICU will require a flat electron beam with a transverse emittance smaller than what has been achieved in round-to-flat beam transformation experiments to date. This program provides additional motivation for extending those experiments.

As shown in Figure 2.3, the ICU consists of two identical metal gratings on either side of the beam vacuum. The electron beam induces its image charge on the metal gratings which apply a Lorentz force (wake field) on the electron beam. Due to the periodic geometry of the gratings, the image charge wake field alternates just like in a conventional magnetic undulator. This process leads to the undulating motion of the electron beam.

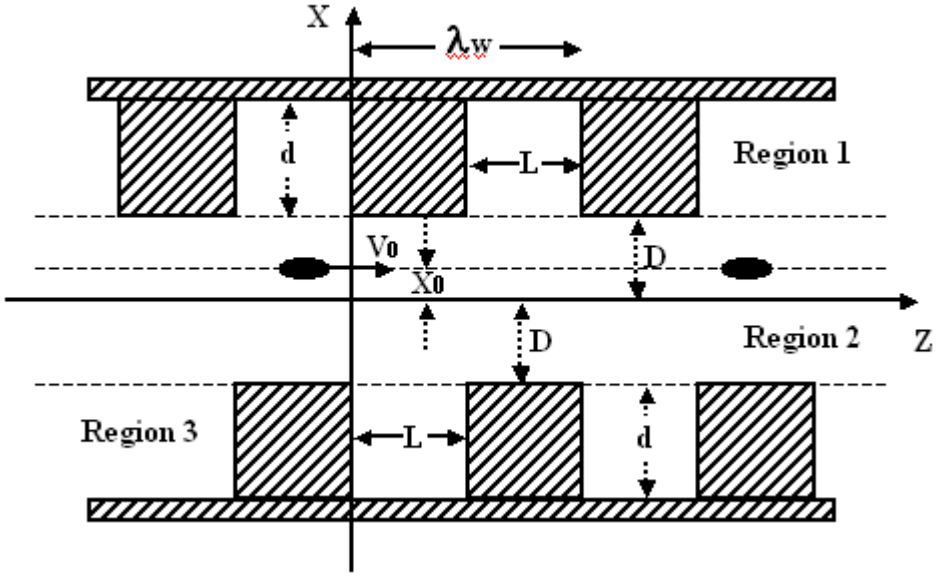

Figure 2.3: Schematic of a 2-D image charge undulator (from ref. [13]).

For a uniform sheet beam and infinitely long undulator, the magnetic field of the image charge wake field has only a non-alternating component which is parallel to the grating groove direction (i.e., B_y only). The vertical electric field near the undulator center is given by

$$E_x(z) = E_0 \sum_{n=1}^{\infty} N_{2n+1} \sin(2n+1)k_w z, \quad E_0 = \frac{\sigma}{2\varepsilon_0},$$

where σ is the surface charge density of the sheet beam, ε_0 is the permittivity of free space, and $k_w = 2\pi/\lambda_w$ is the wave number. The dimensionless coefficients N_{2n+1} depend only on the geometry of the image charge undulator and are given by

$$N_{2n+1} = -\frac{a_n \tanh(2n+1)\pi \dfrac{d}{L}}{(n+\dfrac{1}{2})\pi \sinh(2n+1)\pi \dfrac{D}{L}}.$$

The strength of the transverse electric field is determined by the electron beam charge and size (E_0), as well as the grating geometry (N_{2n+1}). As d approaches 0 (no grating) the image charge force vanishes, and as D decreases the image charge force becomes larger. Keeping only the first term of the transverse electric field, the equation of motion in the vertical direction is

$$v_x(z) \approx \frac{cK}{\gamma}\cos(k_w z); \qquad K = \frac{eE_0 N_1}{mc^2 k_w}.$$

where v_x is the vertical particle velocity. The radiation mechanism follows as in a magnetic undulator, so one may borrow the formulae for the radiation wavelength, spectral and angular distribution of the photons, etc. For example, the radiation wavelength is given by

$$\lambda = \frac{\lambda_w}{2\gamma^2}\left(1+\frac{K^2}{2}\right).$$

For a bunch charge of 1 nC, beam (hardedge) thickness, width, and length of 10 μm, 150 μm, 100 μm, respectively, undulator period of 50 μm, and D/L = 0.5, d/L = 1, the image charge undulator parameter K is about $1.06\text{x}10^{-2}$. The photon angular density of nth harmonic in the central cone N_p^n (in units of photons per second per mrad per 0.1% bandwidth) is given by [15]

$$\left.\frac{dN_p{}^n}{d\Omega d(\Delta\omega/\omega)}\right|_{\theta=0} = 1.74\times10^{14} N_g{}^2 E_e{}^2[\text{GeV}] I[\text{A}] F_n(K).$$

where N_g is the number of grating period, E_e the beam energy, I the current, and $F_n(K)$ is given by

$$F_n(K) = \frac{K^2 n^2}{(1+K^2/2)}\left\{J_{\frac{n-1}{2}}[\frac{nK^2}{4(1+K^2/2)}] - J_{\frac{n+1}{2}}[\frac{nK^2}{4(1+K^2/2)}]\right\}^2$$

Integrating the angular density over the solid angle, we have the number of the photons per second per 0.1% bandwidth given by

$$\frac{dN_p{}^n}{d(\Delta\omega/\omega)} = 1.34\times10^{14} N_g Q_n I(A), \text{ where } Q_n(K) = (1+K^2/2)F_n(K)/n.$$

The bandwidth near the nth harmonic is given by

$$\frac{\Delta\omega}{\omega} = \frac{2.8}{n\pi N_g}.$$

Now consider the first harmonic of the radiation. For an electron beam energy of 30 MeV, a bunch train of 1 nC separated by 1 μs (current = 1 mA), $F_1(K)$ = 1.1 $\text{x}10^{-4}$, a 3.4 cm long ICU will produce $8\text{x}10^9$ photons per second per mrad per 0.1% bandwidth in the central cone at 7.3 nm radiation wavelength, which is about $1\text{x}10^{10}$ photons per second per 0.1% bandwidth integrated over the solid angle. The bandwidth is about 0.1%.

The ICU will require a flat electron beam of suitably small emittance. Over the grating length of 3.4 cm, the beam thickness cannot exceed 2•D, which corresponds to a maximum divergence of about 0.3 mrad. Given a thickness of 10 μm at the ICU center (waist), this corresponds to a normalized emittance of about 0.05 μm for a $\beta_0 \sim 1$ cm. This is ~1/8 of the normalized emittance achieved in round-to-flat beam transformation experiments to date, which were performed at half the charge proposed here. This set of numerical calculations is listed the "Soft-X" column in Table 2.1, as well as other numerical examples of undulator, beam and photon parameters.

Table 2.1: Numerical examples of the image charge undulator experiment parameters

		Green	DUV	Soft-X
Grating tooth width (L)	μm	500	250	25
Grating tooth depth (d)	μm	500	250	25
Grating separation (2D)	μm	500	250	25
Grating period	μm	1000	500	50
Bunch charge	nC	1	1	1
Beam energy	MeV	16	30	30
Beam length	μm	1000	500	100
Beam width	μm	500	250	150
Beam thickness	μm	100	50	10
Radiation wavelength	nm	510.01	72.54	7.25
Undulator parameter K		6.33e-3	1.27e-2	1.06e-2
Gain length	cm	47.91	22.46	3.40
Grating period in a gain length		479	449	679
Norm. rms vertical emittance	μm	0.40	0.40	0.05
Norm. rms horizontal emittance	μm	3.53	3.53	8.42
Norm. rms round beam emittance	μm	1.19	1.19	0.65
emittance ratio		9	9	170

There are several upgrades that can improve the performance of the round-to-flat beam transformation [16]. This includes the upgrade of the RF gun to one with an axial symmetric coupler – which reduces the degradation of the flat beam transformation from the gun asymmetry. More importantly, if the upgraded RF gun can be operated at higher gradient, this will help mitigate the space charge force, which is the major degrading factor in the round-to-flat beam transformation. If an additional capture cavity is available, the beam energy can be further increased to about 40 MeV. Apart from further reducing the space charge force, this upgrade will also make it possible to obtain higher photon energy and larger photon flux. Furthermore, if the flat beam can be compressed through a magnetic bunch compressor, the higher peak current can give rise to a larger image charge force, which will enhance the image charge undulator strength. In this case, the addition of a new dipole mode cavity will provide an improved bunch length measurement. Another procedure that will improve the flat beam quality is the more precise alignment of the skew quadrupoles.

The numerical example for an ICU given here is a 2-D model with an infinitely long sheet electron beam. In fact, the beam transverse and longitudinal distributions will influence the process. There are other theoretical models [17] that treat an axially symmetric wake field undulator that can be adapted to study our planar case.

2.3 Ring beam generation

The generation of ring beams has several potential applications in beam physics. First, ring beams can be used in beam-driven collinear acceleration such as dielectric wakefield based on a cylindrical symmetric structure [18][19]. In this scheme a high charge drive hollow beam excites the wakefield in the dielectric structure and a probe beam propagating on the structure axis is accelerated. In the past, such attempts at low energy resulted in an instability that prevented the scheme from properly working. Therefore the generation and transport of high charge hollow beams is an interesting topic that could be pursued at A0.

On another hand such ring beams, if properly manipulated, might result in very bright beams since for the same charge, a ring beam has a lower charge density than its counterpart uniform cylindrical beam. We therefore conjecture that the transverse phase space dilution due to space charge would be mitigated and if a proper transformation capable of converting this hollow beam into a uniform beam would be implemented at high energies, the final beam could have higher brightness than otherwise achieved. A possible manipulation consists in producing a magnetized ring beam (by immersing the cathode in an axial magnetic field) and using the round-to-flat beam transform to create a beam with one hollowed transverse phase space. A method to coalesce this hollow phase space into a single-peaked phase space distribution was first suggested by Derbenev [20] and one implementation was recently worked out [21][22].

2.4 Microbunching, laser beam heating, and optical replica

Over recent years there has been considerable study of possible microbunching processes in linacs that provide short bunches with high peak current for FEL application. These linacs have magnetic bunch compression that can convert energy modulation to charge density modulation after the compressor. High frequency components in the beam can result from coherent synchrotron radiation (CSR), wakefields, and longitudinal space charge (LSC) effects. In particular modulation in bunch charge can provide energy modulation through space charge that then can be amplified in the compressor resulting in further charge modulation at higher frequency due to compression. Such an effect was initially hinted by start-to-end simulation of LCLS and a theory was developed in Reference [23]. Because of the possibility of this effect, the XFEL has incorporated a “laser heater” to be able to increase the uncorrelated energy spread.

This beam microbunching has caused unexpected enhancements of the beam images from optical transition radiation (OTR) beam profiling screens. This has been observed at LCLS [24], APS [25], and FLASH. The ultra low emittance beams at a small focus exceed the threshold for YAG:Ce scintillator linearity, so OTR screens are indicated. However, following bunch compression there seems to be a combination of LSC and CSR induced microbunching that results in these coherent OTR (COTR) emissions nonuniformly fluctuating over the beam image. The LCLS is presently precluded from using their OTR screens from 135 MeV to 14.3 GeV to perform reliable beam profile and hence emittance measurements. Besides the diagnostics complication there may be a contribution to the emittance degradation in the chicane bends from COSR and FIR CTR. Examples of the data taken at APS are shown in Figure 2.4 where the almost 10 times more intense spikes show up near maximum compression in the image and profile at the right.

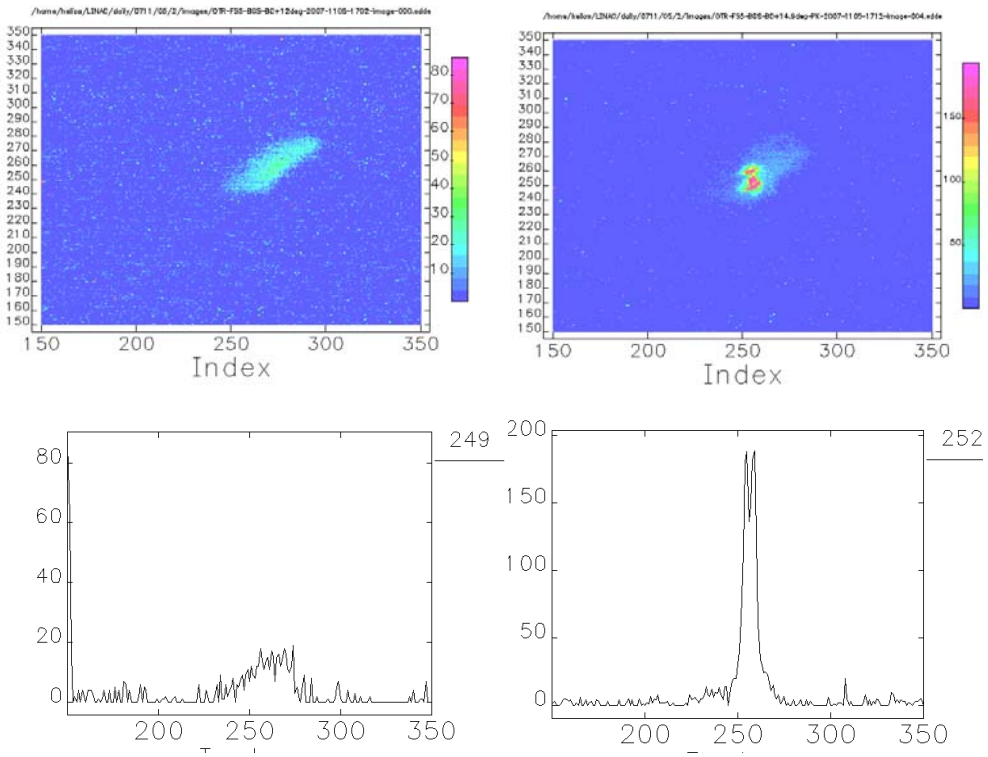

Figure 2.4: Comparison of the OTR images obtained after the chicane at low compression (top left) and high compression (top right). The corresponding x profiles through the images are shown in the two lower plots. The enhancement is about a factor of ten in the profile on the right.

What seems to surprise people is that this coherent effect shows up in optical frequencies and there is speculation as to the generation mechanism [26]. It is not known if these fundamental LSC effects will be evident at 40 MeV following bunch compression of the bunches to sub-500 fs FWHM bunch lengths. However there is speculation by Rosenzweig that freezing space charge is important and that we may not be at high enough energy. Currently, we only compress in the dogleg configuration at A0, and we have not yet seen the effect in our brief inspections of the beam images. We plan to reinstall a compressor in the straight ahead line that will make possible observation easier. Initial measurements and modeling would look for the effect and how to possibly generate it by inducing bunch modulation. . We suspect that the emittance exchange experiment at A0 will also be an interesting test on the microbunching effect. If the effect can be observed, further studies and modeling of it and its mitigation would be warranted. The understanding and mitigation of this effect has become a critical task for LCLS, Elettra, and other advanced accelerators. It has been one topic of this year's Zeuthen CHBB Workshop in May 2008.

The laser heater concept [27] involves the co-propagation of a laser beam and e-beam through a short undulator section as shown in Figure 2.5a. This is now planned for LCLS at 135 MeV to suppress CSR effects [28]. This same heater process should lead to damping of the LSC effects as well. If this is true, then the OTR screens would be usable again after bunch compression

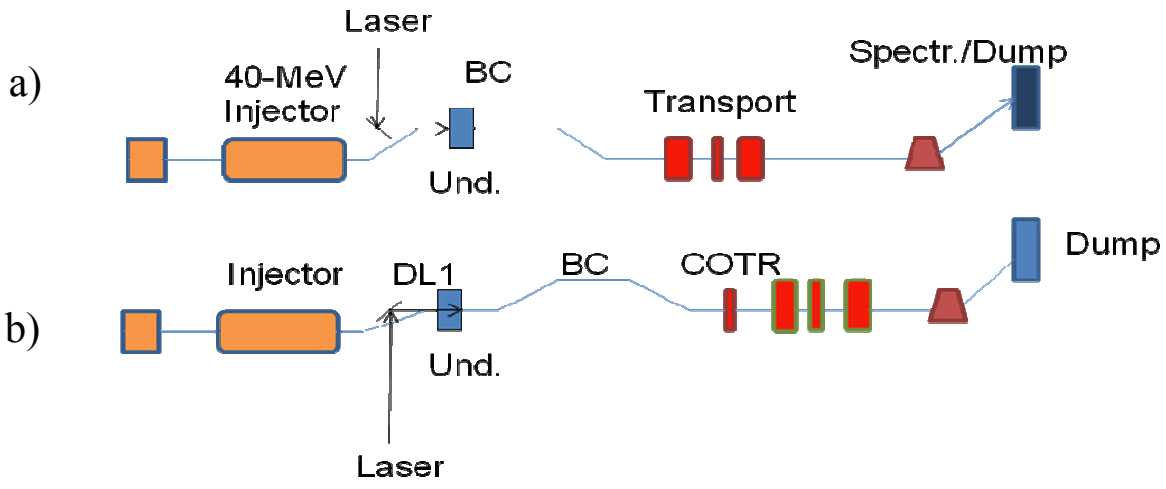

Figure 2.5: Schematics of (a) a laser heater configuration (b) and optical replica configuration at the A0 upgrade bunch compressor.

Recently FLASH has demonstrated results from an Optical Replica Experiment [29]. Here, the laser e-beam interaction in the undulator could be done before the chicane to induce energy modulation at the 780 nm wavelength which becomes microbunching after the chicane. This mode is shown in Figure 2.5b. The exciting prospect is that one could use a short laser pulse to microbunch a slice of the x-y cut and then obtain slice beam size information as shown in Figure 2.6. If one uses a laser pulse longer than the e-beam than the longitudinal profile could be obtained from the COTR with a streak camera or FROG (frequency-resolved optical grating) with 100 fs resolution.

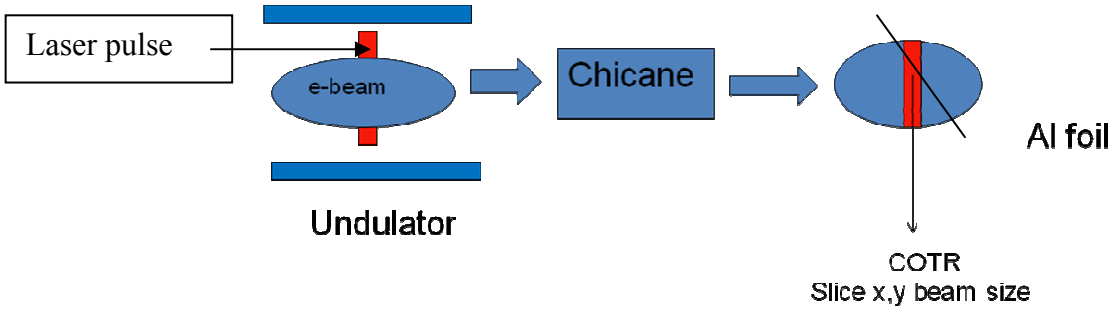

Figure 2.6: Schematic of the optical replica mode for obtaining slice beam size information with 100 fs sampling.

The microbunching effect is another way to address the lower OTR signals for lower-energy beams. The coupling of our microbunching experience from other past experiments with the optical replica technique and the laser heater are logical extensions [25][30].

Both the heating and Replica require a laser synchronized with the gun drive laser. The estimated energy is ~1 mJ/bunch. Typically a wavelenth of ~ 775 nm is used. We need to evaluate just what such a laser would be and its cost. Having a laser system to interact with the beam would enhance our ability to carry out a variety of experiments and instrumentation development. It is

possible that such a laser could be used for inverse Compton scattering at low intensity as well (see section 2.5).

2.5 Inverse Compton scattering

Inverse Compton scattering is being studied at other laboratories [31]. Even so, the potential for this type of compact source to provide high flux and brilliance x-rays for users at small facilities makes it an important technology to try to help develop. Potential applications include time resolved experiments in the ps range, protein crystallography, and phase contrast imaging [32].

The A0 Photoinjector has many features in common with a possible future source, but it also is lacking in some fundamental ways. With that said it still could provide a stepping stone in technology and testing toward what might be constructed as a real 1st generation facility of this type.

The key features of an envisioned compact facility are: a SRF gun , a CW SRF linac of ~ 20-30 MeV, a bunch compressor, and a very high Q laser cavity. Very good beam emittance, quality, and stability are required. The typical bunch repetition rate and charge would be 10 MHz and 100 pC. Development is needed for a cost effective linac and gun system, and for the high Q laser cavity.

However at A0 there is the potential for testing at the level of few bunches/sec the production of the inverse Compton x-rays in the 12 kV energy range and understanding just how to control the low beta interaction parameters to supply brightest peak (photons/sec mm^2 mrad^2 0.1%bw) and average (photons/sec mm^2 mrad^2) brightness for the electron beam and laser energy available.

One goal would be to use a relatively low power laser (such as mentioned above for microbunching control) and develop and investigate the system and beam parameters such as to achieve the best possible spectral brightness. This is dominated by electron beam divergence at the photon interaction point and so it would be strongly related to the gun emittance and bunch charge as well as the optics and stability at the interaction region. This demand for low emittance ~ 1 mm-mrad could well drive us to the exploration of the pancake type gun laser beam and ellipsoidal electron bunch development. For any integrated system study, timing synchronization at the 100 fs level will need to be developed.

Another goal that would go further toward final parameters would be to have a prototype high Q, high energy/bunch laser to integrate into the injector system and test this integrated system. The type of laser that is being contemplated is of a compact design at 1 μm wavelength with an eventual drive power of 5 kW and a cavity power 1000 times greater. A first generation system for low repetition rate would be much less demanding.

We believe that to undertake this exacting type of systems test we would need a particularly interested collaborating group that would bring laser expertise, and possibly a laser, as well as personnel.

References

[1] Y. Orlov *et al.*, CLNS Report 91/1092 (1991); CBN Report 91-9 (1991).

[2] M. Cornacchia, P. Emma, Phys. Rev. ST Accel. Beams **5**, 084001 (2002).

[3] K.-J. Kim, A. Sessler, in *AIP conference Proceedings **821***, p 115.

[4] D. Edwards, *Note on transit in deflecting mode pillbox cavity*, WWW Document, (http://nicadd.niu.edu/aard/emittance_exchange/dae20aug20.pdf).

[5] P. Piot, in *Proc. 13th Advanced Accelerator Concepts Workshop, Santa Cruz, CA* (2008, to be published).

[6] M. Dohlus, T. Limberg, *CSRtrack Version 1.2 User's Manual*, WWW Document, (http://www.desy.de.xfel-beam/csrtrack/).

[7] S. G. Anderson, *et al.*, Phys. Rev. Lett. **91**, 074803 (2003).

[8] F. Zhou, *et al.*, Phys. Rev. ST Accel. Beams **9**, 114201 (2006).

[9] M. Dohlus, T. Limberg, in *Proc. PAC2005, Knoxville, TN*; M. Ferrario *et al.*, TESLA-FEL Report 01-03 (2001); F. Stulle, Ph.D. thesis, University of Hamburg (2004).

[10] G. Andonian, TUBMS033, in *Proc. PAC2007, Albuquerque, NM*.

[11] P. Piot, Y.-E. Sun, M. Rihaoui, in *Proc. 13th Advanced Accelerator Concepts Workshop, Santa Cruz, CA* (2008, to be published).

[12] Y. Zhang *et al*., in *Proc. FEL2002, Argonne, IL*.

[13] Y. Zhang *et al.*, in *Proc. PAC2003, Portland, OR*, p. 941.

[14] P. Piot *et al.*, Phys. Rev. ST Accel. Beams **9**, 031001 (2006).

[15] K.-J. Kim, Eq. (4.44) in practical units, in *AIP Conference Proceedings **184***, p. 600.

[16] Y.-E. Sun *et al.*, in *Proc. PAC2005, Knoxville, TN*, p. 3774.

[17] A. Opanasenko, in *Proc. EPAC2004, Lucerne, Switzerland*, p. 2415.

[18] P. Shutt, in *Proc. All-union Conference on New Methods of Charged Particle Acceleration*, (Springer, NY 1989).

[19] J. L. Hirshfield, in *Proc. 13th Advanced Accelerator Concepts Workshop, Santa Cruz, CA* (2008, to be published).

[20] Y. Derbenev, NIM A **441**, 223 (2000).

[21] S. Nagaitsev, Mathcad simulation program, private communication (July 2008).

[22] D. Edwards, M. Syphers, "Comments on an Experiment on Transverse Coalescing" (unpublished).

[23] E. Saldin *et al*., TESLA-FEL Report 2003-02 (2003).

[24] R. Akre *et al.*, Phys. Rev. ST Accel. Beams **11**, 030703 (2008).

[25] A.H. Lumpkin, *et al*., "Observation of Enhanced OTR Signals from a Compressed Electron Beam", in *Proc. BIW2008, Lake Tahoe, CA* (to be published).

[26] J. Rosenzweig, in *Proc. 13th Advanced Accelerator Concepts Workshop, Santa Cruz, CA* (2008, to be published).

[27] E. Saldin *et al.*, NIM A **490** (2002).
[28] Z. Huang *et al.*, Phys. Rev. ST Accel. Beams **7**, 074401 (2004).
[29] G. Angelova *et al.*, in *Proc. EPAC2008, Genova, Italy*, p. 1332 (to be published).
[30] A.H. Lumpkin *et al.*, PRL **86**, 79 (2001).
[31] W. Brown *et al.*, Phys. Rev. ST Accel. Beams **7**, 060702 (2004).
[32] D. Moncton, *et al.*, *MIT Compact X-ray Source,* MIT White Paper, (unpublished).

3 Advanced beam instrumentation

Besides the measurement of fundamental beam parameters (intensity, position, transverse size and emittance) the experiments proposed at A0 require advanced instrumentation to observe in detail the longitudinal characteristics of the bunches. Therefore most of the proposed plans for advanced beam instrumentation focus on longitudinal beam parameter characterization: bunch length, bunch profile, and bunch time-of-arrival (wrt RF phase). Each of the presented methods has its particular pros and cons; none is able to fully characterize the longitudinal bunch parameters perfectly in a single shot, non-invasive manner. The instrumentation capabilities are summarized in Table 3.1.

Table 3.1: Bunch length measurement devices with the applicable ranges and features of each.

Device	Applicable Bunch Lengths	Comments
Streak Camera	> 1-2 ps	Well understood, expensive, commercial device which does single bunch Dispersion effects dominate short bunch length measurements Can provide arrival times and jitter
Martin-Puplett Interferometer	< few ps	Slow response; scanned over many macropulses Susceptible to upstream CSR and wakefields Missing phase makes details of bunch profile difficult to obtain
CTR angular distribution	< few ps	Parametric measurement of bunch profile; must input assumed shape Scanned over many macropulses Susceptible to upstream CSR and wakefields
Electro-optical Sampling	100 fs – 2 ps	Single shot, fairly expensive as it requires a laser synchronized to the beam Must understand behavior of electro-optical crystal in frequency regime corresponding to expected bunch lengths Susceptible to upstream CSR and wakefields (less so than CTR and M-P Int.)
Waveguide Pickup	200 fs – 2 ps	Inexpensive and simple, but absolute calibration is very difficult. Does not give shape, just rough bunch length

3.1 Ongoing development

3.1.1 Streak camera

Introduction

The opportunity for a new series of streak camera experiments at the A0 photoinjector was recognized in the last year. The enabling upgrade was adding the synchroscan option to the existing C5680 Hamamatsu streak camera mainframe. By locking this module to the 81.25 MHz subharmonic of the RF system, the synchronous summing of bunches could be done with a trigger jitter of <1.5 ps FWHM for both the UV drive laser component and the e-beam via optical transition radiation (OTR) measurements. The synchronous summing of the low OTR signal from the 15 MeV e-beam bunches allowed the needed bandpass filters to be utilized to reduce the chromatic temporal dispersion effects inherent to the broadband OTR source and the transmissive optics components. In addition, the C6768 delay module with phase feedback was also acquired, and this stabilized the streak camera sweep relative to the master oscillator so that the camera phase drift was reduced to the picosecond level over tens of minutes. This latter feature allowed a series of experiments to be done on the bandwidth effects and transit time effects in the respective transport lines, including evaluation of the matrix elements of the emittance exchange line.

In the course of our experiments, we have done a series of tests on the chromatic temporal dispersion effects for this particular input optics barrel with UV transmitting optics and our optical transport lines. Our effects are less than that reported at SSRL with optical synchrotron radiation [1], but our results still need to be characterized carefully to allow accurate bunch length measurements using the OTR. In Fig. 3.1 we show our correction curves for the two streak camera ranges, R2 with 1.55 ps/pixel and R1 with 0.32 ps/pixel. We will use a 550 nm longpass filter as a compromise on effective bandwidth and the reduced variation in group velocity with wavelength in the red end of the spectrum. This results in a contribution to system time resolution of about 2.6 ps FWHM due to this bandwidth effect including a quartz window, one quartz lens, and the input optics barrel. The optics barrel lens set is the largest contributor. The intrinsic tube resolution for a single wavelength is 1.5 ps FWHM (0.6 ps σ). The R2 range should generally be used for bunch lengths longer than 8-10 ps. At the shortest bunch lengths the sensitivity to changes becomes reduced as one works near the system resolution value as shown in the R1 curves.

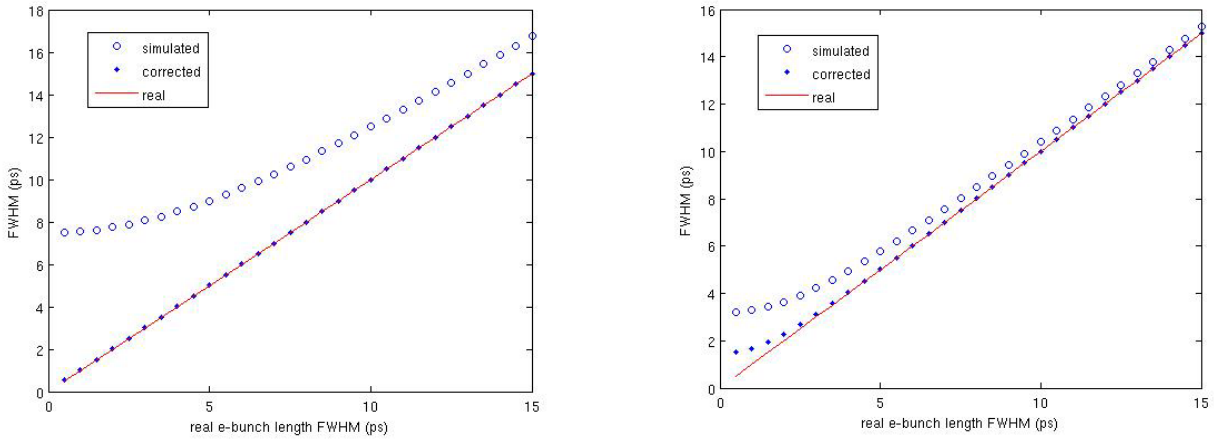

Figure 3.1 Comparison of actual bunch length (red) versus the simulated effects of camera resolution and bandwidth (circles) for R2 (left) and R1 (right) and our corrections (dots) based on subtraction of the relevant terms in quadrature. The 550 nm longpass filter was assumed.

After characterizing the UV laser bunch length, a series of e-beam experiments on the A0 beamlines was performed [2]. We have measured a significant bunch length elongation versus bunch charge for the present conditions in the uncompressed line (blue line) and show that this is consistent with ASTRA calculations (black line) in Figure 3.2. The green line shows data taken in 2005 using a different laser spot size on the cathode. We also observed a time-dependent transverse focusing effect at 4 nC/bunch as shown in Figure 3.3. Such a "self-pinching" effect is observed in typical high charge bunch simulations. Our experiments indicate the bunch head and tail to have 50% larger transverse size than the bunch central slices. The bunch length is 28 ps FWHM. This topic merits further study in FY09: detailed beam dynamics simulations using particle-in-cell calculation will be performed and the evolution of the (x,t) configuration pattern will be studied for different electron source settings (solenoids, and laser (flat top versus Gaussian distribution).

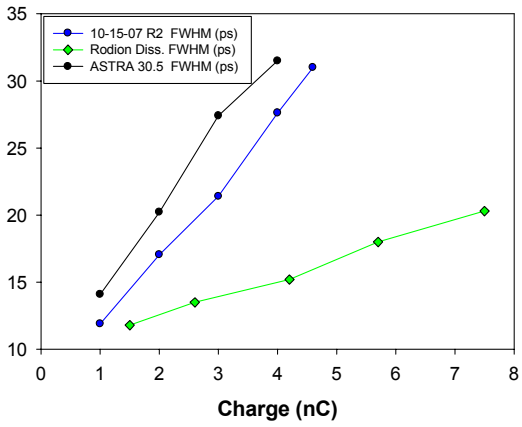

Figure 3.2: Comparison of the variation of bunch length FWHM with bunch charge (blue curve). Vertical axis is in ps.

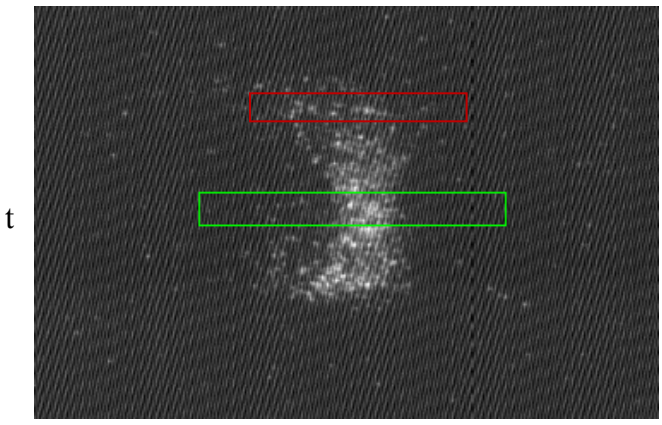

Figure 3.3: Evidence of time-dependent transverse focusing effects in a 4 nC bunch.

Additionally, we report measurements of the bunch compression in a double-dogleg transport line as a function of the upstream 9-cell accelerator RF phase in Figure 3.4. The observed bunch length varies from 22 to 4 ps FWHM as shown. The simulated bunch length is 3.5 ps FWHM at maximum compression. The cross-comparison of our compensated bandwidth effects on the two fastest sweep speeds, R2 and R1, are also shown for the R2-550 nm shortpass filter (red), R1-550 nm shortpass filter (green) and R1-550 nm longpass filter (black) data. The overlaps of the curves at common phase settings are good cross-checks.

The trajectory change with beam energy can be studied via the transit time changes through the doglegs as shown in Figure 3.5. The phase-locked streak images allow the change in image time position to be used to track the arrival time change. One can see that a ±1% change in momentum causes about ± 6 ps change, respectively, in transit time through the bends. These data were used to evaluate one of the transport matrix elements of the emittance exchange line.

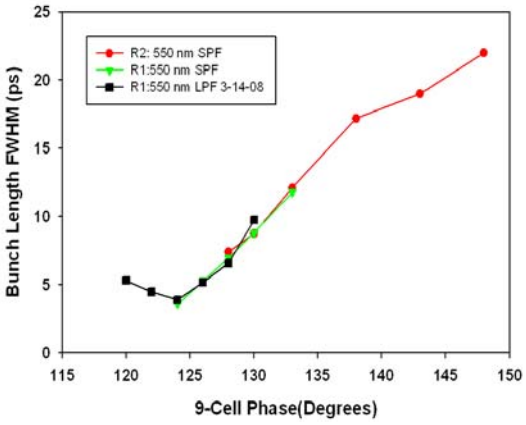

Figure 3.4: Bunch compression versus 9-cell phase. The expected bunch length is 3.5 ps FWHM at maximum compression.

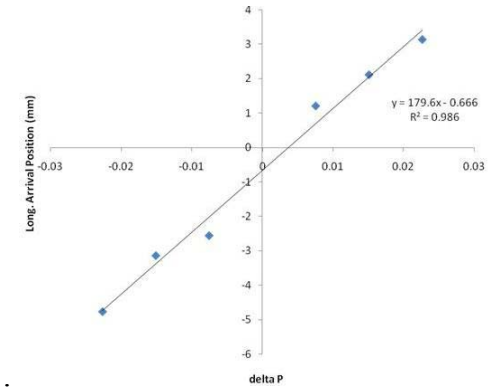

Figure 3.5: Transit time through the doglegs for different momentum changes. The line is a fit showing that R_{56} is 0.18 m

One of our more critical measurements this year was the verification of the x-z emittance exchange process by graphically showing the reduction in the bunch length when the 5-cell cavity is at 100% power compared to power off. This is shown in Figure 3.6 where the horizontal axis is in seconds, or shot number, for each state of the cavity power, and the vertical axis is the corrected bunch length. The FWHM length reduction from 5.2 ± 0.7 ps to 1.2 ± 0.8 ps is clear. Note however that the 1.2 ps number is well below the resolution shown in Fig 3.1 so its absolute value may have large systematic errors.

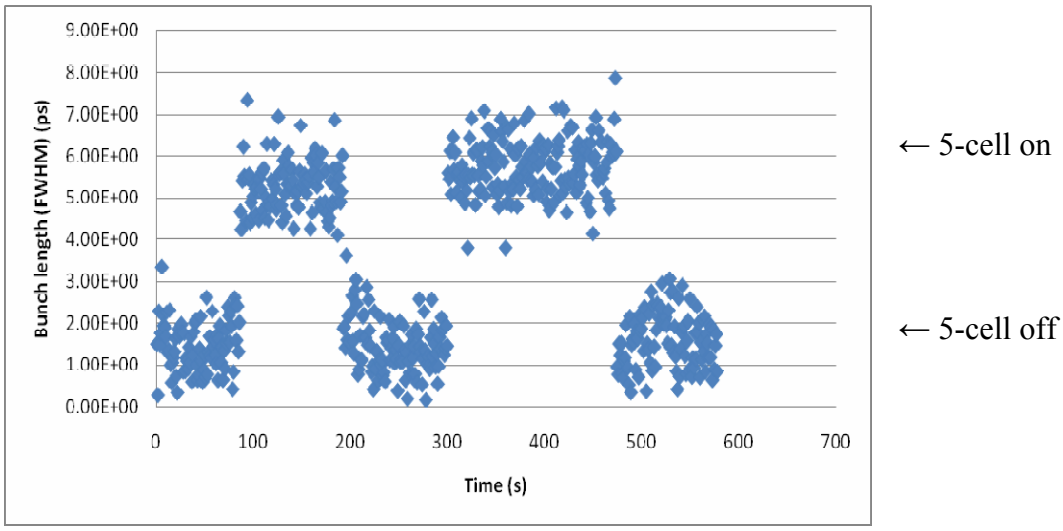

Figure 3.6: Direct measurement of the x-z emittance exchange and the bunch-length reduction with the 5-cell cavity power on versus power off.

Plans

We have just started our dual-sweep streak camera experiments to look for phase jitter and slew within the laser and e-beam bunches. We expect to continue our efforts to reduce the chromatic temporal dispersion effects by testing a grating pair as a compensator or by acquiring a commercial mirror-input-optics assembly for the camera. If either is successfully employed, we can reduce the effective system resolution limit by a factor of ~2 and be able to use 4 times more bandwidth of broadband OTR to improve image statistics. We are also evaluating purchase of a new 12-bit digital readout camera for the streak camera. The combination of these features will bring us closer to single bunch longitudinal profile measurements at the 1 nC level at A0 upgrade energies and will enable slice-emittance tests. The system could support any future x-z emittance exchange experiments, laser/e-beam relative phase tests, and bunch compression tests in FY09 and later. We also could support qualification of the Martin-Puplett interferometer and the CTR angular distribution bunch length measurement methods that are just underway or planned.

The optical transport line will be redesigned to increase OTR signal collection efficiency and allow us to observe the drive laser in the same streak image with the OTR. The direct relative phase information (peak centroid positions) should be obtainable at the 300 fs level -- one camera system pixel. With dual-sweep mode, we should be able to investigate sub-bunch transients and accelerator phase feedback loop issues.

The streak camera system is currently used routinely for beam characterizations and in the x-z emittance exchange experiments. With the proposed upgrades, it can continue to be the reference longitudinal profile and phase measurement device at the 1-2 ps level. It can be used in the development and commissioning of the other techniques that will push measurement capabilities towards the 100-300 fs level.

3.1.2 Martin-Puplett interferometer

One method for determining the bunch length of an electron beam is autocorrelation interferometry. Interferometric bunch length measurements are possible because of the

correlation between the bunch length and the spectral content of Coherent Transition Radiation (CTR) from the bunch. This relationship is formally

$$I(\omega) = I_0(\omega) \cdot \left(N + N(N-1) \left| F(\omega) \right|^2 \right)$$

where $I_0(\omega)$ is the single particle spectrum, and the complex form factor, $F(\omega)$, is the Fourier Transform of the longitudinal charge distribution

$$F(\omega) = \frac{1}{Q} \int dz \, \rho(z) \, e^{-i\omega z}$$

where the transverse contributions are small, provided the observation point is close to the emission axis, and have been ignored.

Notice that the intensity is a function of only the magnitude of $F(\omega)$ and as such, in general, an exact determination of the longitudinal charge distribution cannot be obtained. However, for certain simple shapes, such as Gaussians, the approximations necessary to obtain the phase values do a fairly good job of preserving the main parameters of the bunch, such as width.

At the A0-Photoinjector we have installed a Martin-Puplett interferometer borrowed from DESY (Fig. 3.7). A Martin-Puplett interferometer is a polarizing type interferometer which in this case uses closely spaced wire grids for the polarizers and splitters. The grids consist of 15 μm diameter gold-plated tungsten wires spaced by 45 μm.

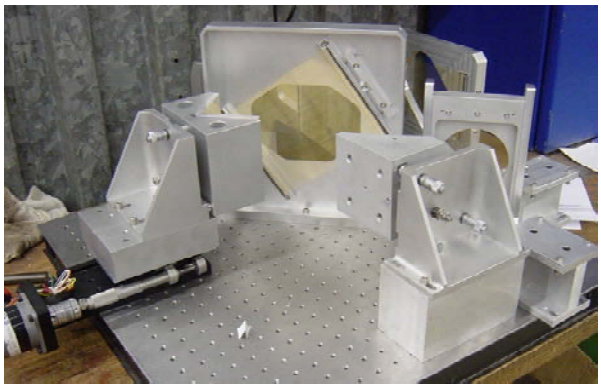

Figure 3.7: Photograph of the interferometer. The gold-colored portion is the wire grid beam splitter.

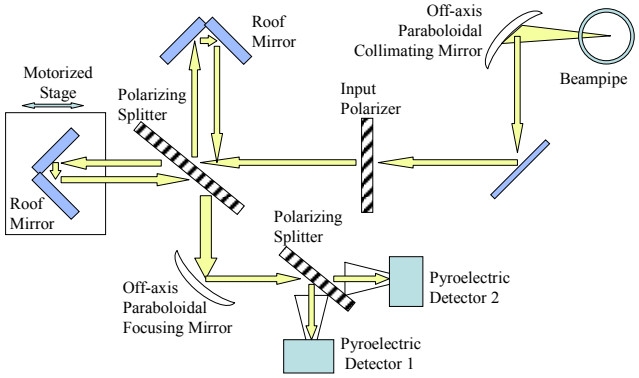

Figure 3.8: Schematic of the interferometer.

The CTR exits the beamline through a quartz window and is immediately collimated by a 200mm focal length off-axis parabolic mirror (Fig. 3.8). Another flat mirror directs the light into the interferometer and through the horizontal input polarizer. The wave is then split by the beam splitter, which is oriented diagonally, into two orthogonal polarization which then traverse their respective arms and arrive back at the beam splitter with a phase difference, $\omega\tau$, which depends on the path length difference. The path length difference is controlled by a motorized stage on which is mounted one of the roof mirrors. The right angle roof mirrors adjust the polarization of the light such that what got transmitted (reflected) at the splitter now gets reflected (transmitted)

so that it can be properly recombined. The recombined wave is then focused and split into horizontal and vertical polarizations, each of which are directed to a pyroelectric detector. The average intensity seen by each detector is

$$I_h(\omega,\tau) \propto \frac{E_0^2}{2}\cos^2\left(\frac{\omega\tau}{2}\right)$$

$$I_v(\omega,\tau) \propto \frac{E_0^2}{2}\sin^2\left(\frac{\omega\tau}{2}\right)$$

The sum of the intensities seen by the two detectors is proportional to the total intensity after the initial input polarizer. Defining the interferogram, S(τ), to be the intensity difference divided by the sum and generalizing to an arbitrary wave by Fourier composition, the interferogram is

$$S(\tau) = \frac{\int d\omega\, I(\omega)\cos(\omega\tau)}{\int d\omega\, I(\omega)}$$

which is the real part of the Fourier Transform of I(ω).

A complication in this technique is the fact that due to the small size of the CTR screen (1.25 cm radius), there is a strong diffraction effect which in turn introduces a frequency-dependence (broadening) of the angular distribution (Figure 3.9). The extent of this broadening depends on γλ.

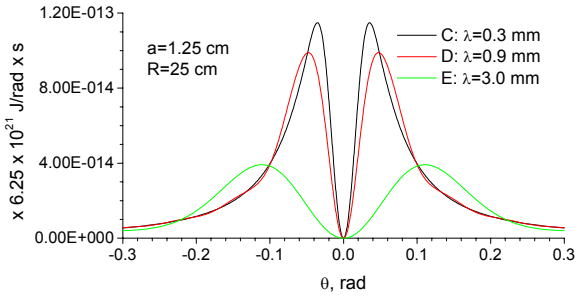

Figure 3.9: Near field angular distribution of different wavelengths of transition radiation at a distance of 25 cm from the CTR screen. Combined with a finite aperture, this effect imposes a frequency dependence on the observed radiation.

Combined with the finite aperture, this leads to a reduction in long wavelengths in the interferogram. A careful calculation can correct for this, but requires a simple geometric shape for the CTR radiator. There is already a plan to replace the existing radiator with a simpler shape. Another issue with this system is the lack of knowledge of the spectral response of the detectors and possible interference effects. We are currently testing a broadband Schottky diode detector as a possible replacement for the pyroelectric detectors.

Comparison of Streak Camera and M-P Interferometer Results

Initial comparisons of the Martin–Puplett Interferometer with the streak camera were made on 6/18/08 (Figure 3.10). The streak camera data used a 40 bunch synchronous sum, and the interferometer scans were done over tens of minutes. The data involved the power cycling of the 5-cell cavity which, because of the x-z exchange, compresses the bunch length, but increases the

horizontal transverse beam size and divergence. This change in the horizontal emittance may have an impact on the measurement. The ratio of 5-cell on/off measurements was 0.66 for the bunch length from the streak camera, 0.69 for the interferometer autocorrelation peak width, and 0.43 for the reconstructed interferometer bunch lengths. The minimum bunch length was 3.7 ps (FWHM) as measured by the streak camera on that day.

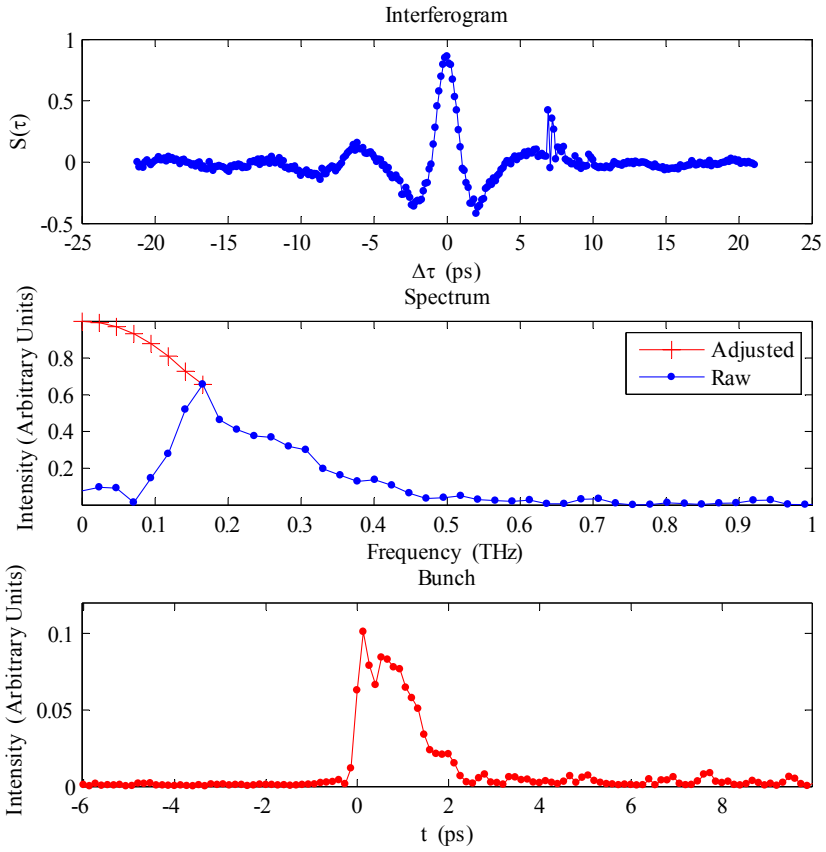

Figure 3.10: Autocorrelation trace (top), raw spectrum (middle blue), corrected spectrum (middle red), and reconstructed bunch (bottom) from 5-cell on/off data.

3.1.3 Electro-optical modulator for time-of-flight measurement

The stability of accelerators depends on the synchronization between the beam, low-level RF, and other accelerator components. A precise measure of the bunch time-of-arrival (TOA) with respect to the master oscillator clock signal is important. Operation of future accelerators places a requirement of measuring the bunch TOA to an accuracy of better than $1/10^{th}$ of a degree of the RF. This results in a need to measure TOA at a resolution better than a few 100 fs. Precision measurement experiments at the A0 photoinjector require bunch TOA measurements to the same resolution.

A bunch TOA monitor with a few 100 fs resolution is in development at the A0 photoinjector and is based on a system developed at DESY [3]. The monitor is based on conversion of time to voltage for amplitude modulation of a pulsed laser via Electro-Optical Modulation (EOM). Figure 3.11 shows the basic principle of the bunch TOA monitor. The zero-crossing voltage of a broadband beam pickup is used to amplitude modulate a single 100 fs wide laser pulse. Figure 3.12 shows how the zero-crossing voltage changes as a function of the bunch arrival time.

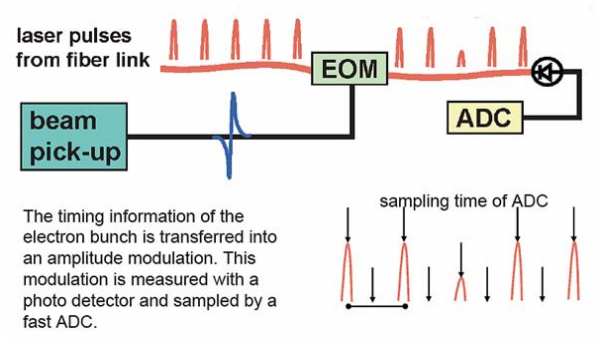

Figure 3.11: Basic principal of the bunch time-of-arrival monitor

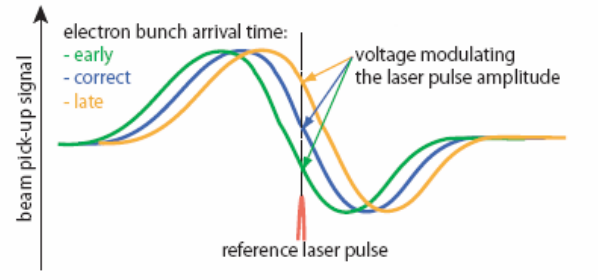

Figure 3.12: Relation between the modulation voltage signal to the bunch arrival time.

Figure 3.13 shows a block diagram of the A0 TOA monitor. A wide bandwidth beam pickup, needed to permit femtosecond TOA measurements, acquires the bunch electric field. Using a precision variable delay line, the pickup signal is timed to arrive at the electro-optical modulator in coincidence with the laser pulse. The zero-crossing of the RF signal is used to modulate the amplitude of a 100 fs wide laser pulse. The photodiode converts the laser pulse into a voltage which is sampled by an ADC.

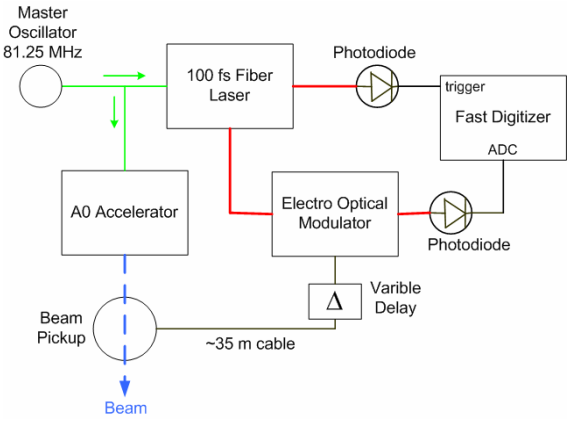

Figure 3.13: Schematic of the TOA at A0.

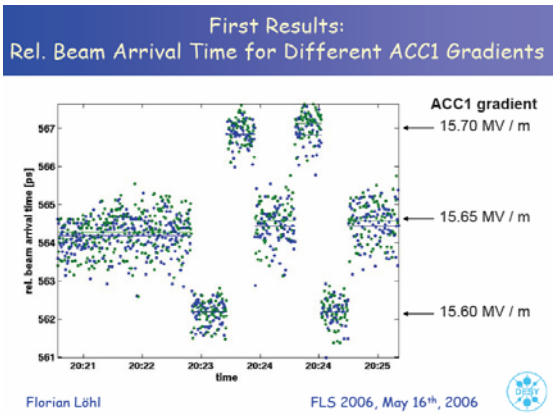

Figure 3.14: First results from DESY FLASH: time-of-arrival vs. accelerating gradient.

A similar monitor has been developed at DESY as a sub-100 fs bunch arrival monitor for the FEL accelerators. Figure 3.14 show the first results from the DESY bunch arrival monitor [4]. These initial results illustrate the potential resolution ability of an EOM bunch time-of-arrival monitor at A0.

3.1.4 Optical transition radiation interferometry

An OTRI technique has been developed to determine the angular spread in the electron beam. The technique employs coherent TR in the optical range generated by single electrons passing through two thin foils separated by a distance of about a coherent length of the TR, which is $\sim\gamma^2\lambda$ for TR of wavelength of λ and beam E/m = γ. The photon phase difference determines the interference pattern which contains information about energy and angular spread in the beam at the given λ. The energy of the beam and the foils separation determine the angular size of the fringes. The characteristics of the fringe contain information about multiple scattering of the electrons in the first foil and beam angular spread. The OTRI apparatus layout and simplified optical scheme are shown in Fig. 3.15 and Fig. 3.16.

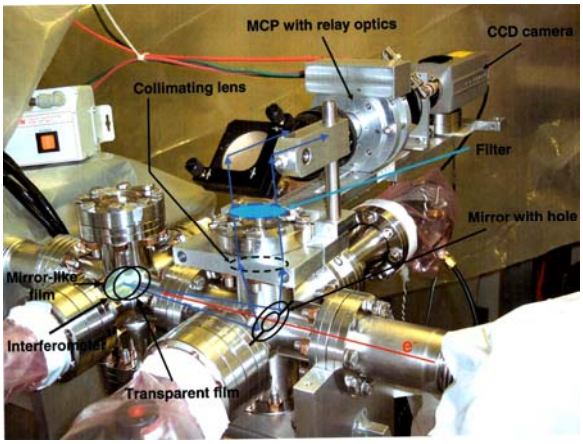

Figure 3.15: OTRI apparatus at A0.

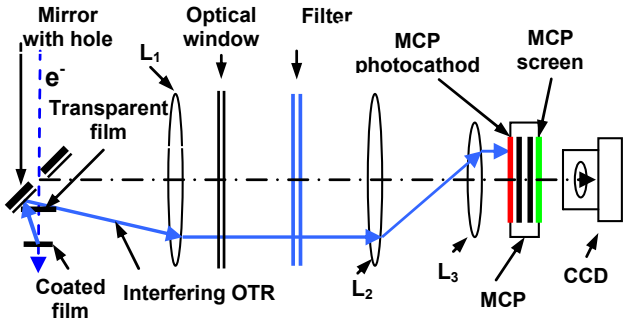

Figure 3.16: The OTRI setup with normal incidence of the electron beam.

We have studied the OTRI pattern obtained with 2.5 μm thick Mylar films and 6 μm thick mica sheets at normal and 45^0 incidence of the electron beam. Fig. 3.17 shows the pattern obtained with 45^0 incidence setup at the beam energy of 16 MeV.

For setup with normal incidence of the electrons, the simulated interference profile coincides with the measured one with an accuracy of few percent for beam angular spread in the range of 1-8 mrad and for the Mylar-based interferometer using 2.5 μm thick Mylar films. For the mica-based interferometer using 6 μm thick mica sheets the agreement is not as good, however we expect that decreasing the mica thickness to 3 μm will provide better agreement between simulation and data.

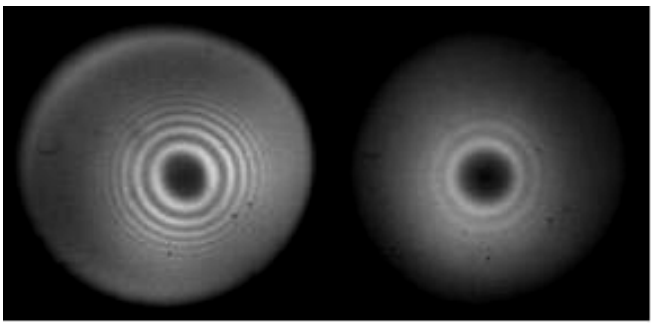

Figure 3.17: The fringes obtained at 45° incidence with Mylar-based (left) and mica-based (right) interferometers.

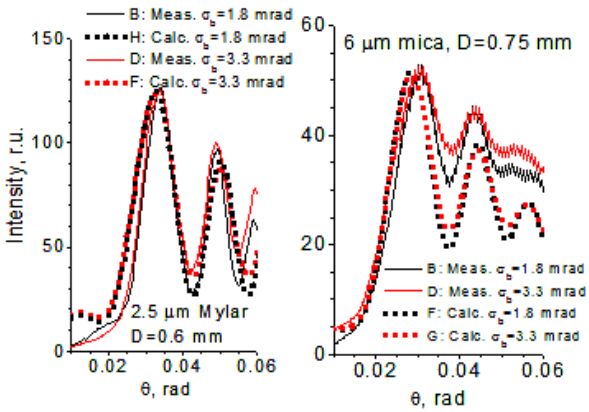

Figure 3.18: Measured (solid lines) and simulated (dotted lines) for Mylar-based (left) and mica-based (right) interferometers at normal incidence.

Plotted in Fig. 3.18 are the measured (solid lines) and the simulated (dots) interference pattern profiles in the setup with normal incidence of 16 MeV electrons. The beam angular spread was also determined by measuring the beam size along the beamline and using the slit technique. The accuracy of this determination is ~16%. Figure 3.19 shows a comparison of beam angular spread as calculated by the OTRI technique and the direct (slit) measurement.

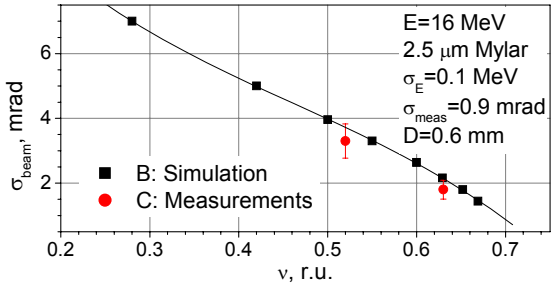

Figure 3.19: Comparison of OTRI calculation of beam angular spread and slit technique of measuring beam angular spread. The visibility, (Imax-Imin)/(Imax +Imin), is plotted in relative units. The error bars on the measurements reflect the uncertainty in the slit measurement.

We have developed the OTRI model taking into account spreads of the electron beam energy and the angles in the beam, the multiple scattering in the interferometer, and resolution of the optical readout. The model gives good agreement with measurements at $\gamma \approx 30$, RMS angle of multiple scattering in the interferometer of ~ 1-2 mrad, and the range of RMS beam angular spread of 1-8 mrad. Increase of the beam energy up to 30-50 MeV makes the OTRI technique preferable in comparison with the slit technique giving good results in the beam divergence measurements at lower energy. Moreover, increasing the beam energy to 30-50 MeV decreases the multiple scattering RMS angle which makes commercially available 3-5 μm thick mica sheets the preferable alternative for the interferometer due to its good vacuum properties.

3.2 Proposals for new development

3.2.1 Longitudinal diagnostics via coherent radiation angular distribution

Coherent transition radiation (TR) and diffractive radiation (DR) spectra have been used to measure bunch lengths of picosecond electron bunches. However the angular distribution of this radiation also contains information on the longitudinal distribution of the bunch. When the size of the radiator, r, satisfies the condition $\lambda \sim 2\pi r/\gamma$ and radiation wavelength, λ, is on the order of the bunch length then the angular distribution of the radiation is very sensitive to the longitudinal distribution of the bunch [5]. Therefore by properly choosing the size of the radiator, for a given beam operating point, one can use the shape of the TR or DR angular distribution pattern to determine longitudinal information.

A flat screen radiator experiment has been proposed by Ralph Fiorito (University of Maryland) for the A0 photoinjector for making such angular distribution measurements. Theoretical models show that a well-defined radiator size allows for a bunch length measurement based on the angular distribution of the coherent TR at A0. The absence of ill-defined diffraction effects due to inaccuracies, screws, holders, etc. is essential for the success of the method. The coherent TR angular distribution will be measured using a highly sensitive Golay cell and a Schottky diode and compared to other A0 longitudinal detectors such as the streak camera (see section 3.1.1) and the Martin-Puplett interferometer (see section 3.1.2).

The advantages of this technique over other longitudinal measurements is that it is simple to experimentally implement, it can be performed at any transition radiation detector location and it can be tuned to measure sub-picosecond bunches. Presently, the measurements will be made with a scanning detector but an array of detectors could be developed to improve the time required for the measurement.

Figure 3.20 shows the calculated angular distribution of coherent TR, using a radiator optimized for current A0 beam parameters, for two different bunch lengths. The simulation shows the clear effect on the angular distribution due to change in bunch length. As part of the A0 upgrade, a radiator optimized for these parameters will be installed.

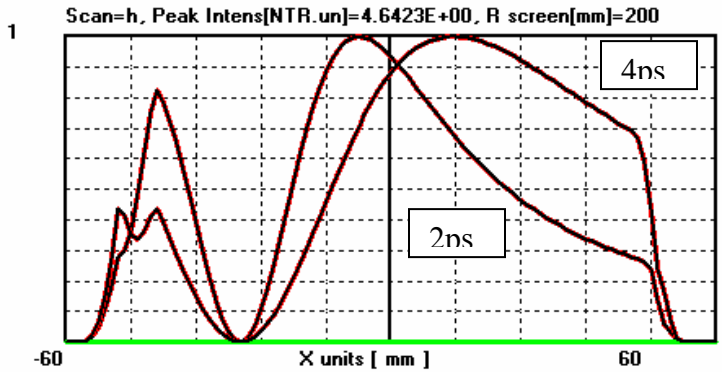

Figure 3.20: Calculated distribution of coherent TR observed from a flat detector plane at distance to source of 200 mm. The simulation is for 16 MeV electrons and Gaussian bunches of 2 and 4 ps width. The distribution is a horizontal scan from an optimized radiator size of 16 X 25 mm at 41 degrees to beam.

Measurements of the angular distribution of coherent TR and DR have been performed at the Swiss Light Source (SLS) at the end of the 100 MeV pre-injector [6]. Figure 3.21 shows the

angular distribution of coherent TR with the theoretical best fit. Calculations show that for a single Gaussian bunch shape the best fit occurs at a width of 0.69 ps. Figure 3.22 shows the same angular distribution but with a double Gaussian bunch shape fit. The best fit occurs for Gaussians widths of 0.57 and 2.84 ps with the second Gaussian shifted by 1.5 ps.

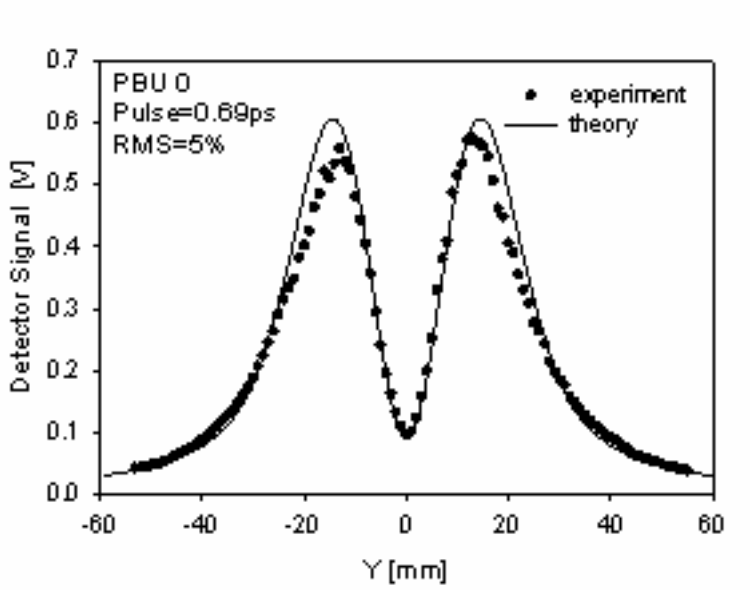

Figure 3.21: Measured coherent TR from 100 MeV electrons at SLS. Theory curve is best fit model based on single Gaussian longitudinal bunch shape.

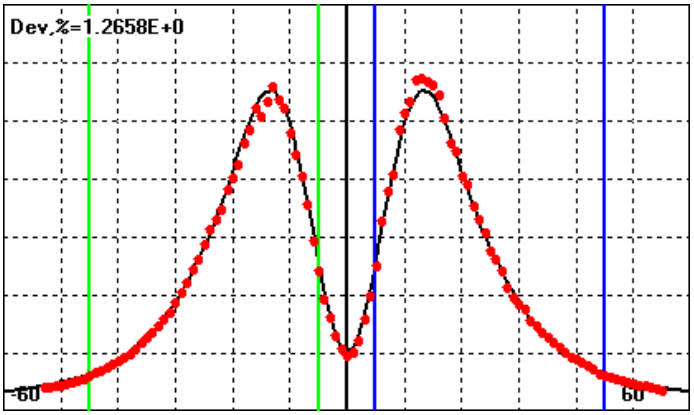

Figure 3.22: Measured coherent TR from 100 MeV electrons at SLS. Theory curve is best fit model based on double Gaussian longitudinal bunch shape.

3.2.2 Electro-optical sampling

Electro-optical (EO) sampling has been proven to be a very effective non-intercepting technique for measuring longitudinal bunch information [7]. We propose that EO sampling be studied with the present A0 photoinjector and integrated into the upgraded A0 accelerator. The goals of EO sampling at A0 are to develop methods not explored at other accelerators and to provide a fully operational diagnostic tool for other A0 experiments. Presently, the unique EO sampling

opportunities at A0 are: (1) measure longitudinal bunch information of low energy electron beams; (2) measure longitudinal bunch information for bunch lengths up to a few ps; and (3) investigate the use of alternate laser wavelengths via fiber lasers. As cross-checks, longitudinal bunch information from EO sampling will be compared with streak camera measurements (see section 3.1.1), Martin-Puplett interferometer measurements (see section 3.1.2), and with the future deflecting mode cavity (see section 4.4).

Currently, most single–shot EO sampling experiments are carried out using either spectral decoding, temporal decoding, or spatial decoding. These three techniques are shown in Figure 3.23. Each technique has unique properties that must be evaluated in terms of the bunch measurement requirements. For example, the best resolution has been reached using the temporal decoding technique, but this technique requires a more powerful laser than spectral or spatial decoding.

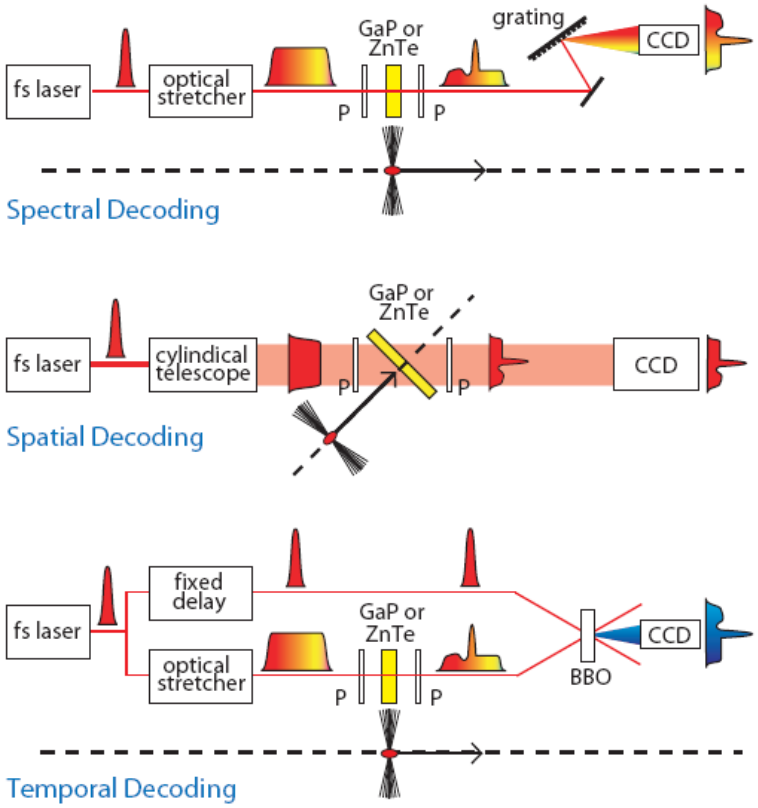

Figure3.23: Schematic representations of the 3 common single shot EO detection techniques [8].

Among the three methods, temporal decoding is able to measure the shortest bunches, spatial decoding has been used as a fs resolution clock at advanced light sources [9], and spectral decoding has been effective in measuring longer pulses. With the current bunch lengths at A0, a spectral decoding method will be as effective as the other methods. For example, Figure 3.24 shows that simulated temporal decoding and spectral decoding signals are identical for a 300 fs (rms) electron bunch.

Our efforts and plans at A0 will concentrate on developing single-shot EO sampling based on the spectral decoding and spatial decoding techniques to investigate low energy electron beams with

bunch lengths 200 to 2000 fs (rms). In addition, current EO studies are focused on high energy beams (few hundred MeV and higher). EO sampling of low energy electron beams has not been studied, and our proposed research will address this low energy gap.

We will also concentrate on developing a suitable fiber laser system for EO sampling. Present EO sampling methods utilize expensive Ti:Sapphire lasers. In addition, transport of the Ti:Sapphire beam to the beamline is problematic. Fiber lasers may solve these problems and make EO methods more convenient and affordable for multiple locations in a large accelerator facility.

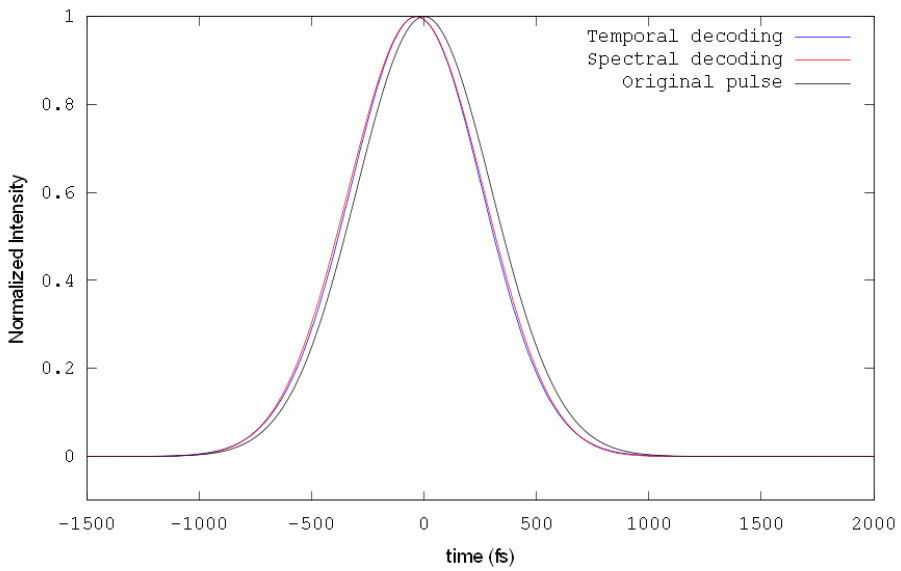

Figure 3.24: Simulation of temporal and spectral decoding signal for a 300 fs rms e-beam using a fs laser pulse at 800 nm.

A0 Current Laser System

The bandwidth of our current Nd:YAG A0 laser system is too small to do an optimal EO experiment, however, this laser can still be used to begin our EO sampling efforts. Because of the longer bunches and limited bandwidth of the Nd:YAG laser, it will difficult to chirp the laser pulses enough to perform spectral decoding, therefore we will do an initial experiment with spatial decoding using the current laser system on long bunches up to a few ps. We expect to accomplish two things in this experiment. First we will learn more detail of the uncompressed A0 electron beam longitudinal structure and compare it to our streak camera measurement. Second we will have in place a suitable optical path and EO beamline device for a future fs laser system (Ti-sapphire or fiber laser).

Ti:Sapphire laser system

A Ti:Sapphire laser is used to generate ultrashort pulses (down to 10's of fs) because of its large bandwidth. To date most EO experiments have used commercial Ti:Sapphire systems, and we also plan to use a commercial system. We have formed a collaboration with Argonne National Laboratory (ANL) and Northern Illinois University (NIU) to study EO sampling

Because of the availability of an amplified Ti:Sapphire laser at ANL, initial EO experiments have been carried out at the Advanced Wakefield Accelerator at ANL. At ANL we have already

used a ps laser pulse to focus on a ZnTe crystal to generate terahertz radiation as measured with a LN_2-cooled Golay cell. In the next stage, an EO setup with a spatial decoding technique will be assembled using parts already purchased. After this stage the setup will be moved into the AWA beamline and experiments with beam will be carried out.

At NIU, a new Ti:Sapphire and amplifying system has been purchased. One graduate student has been assigned to carry out bench-top studies in the NIU laboratory. After these bench-top measurements, the laser setup will be moved to the A0 photoinjector and experiments with the electron beam will be conducted. Both spectral and spatial decoding will be investigated. This work will be a major component of the student's Ph.D. thesis project. In addition, advanced EO studies, such as real-time beam structure and position monitoring, will be carried out using this setup.

Fiber laser system

Although a Ti:Sapphire laser system is the laser of choice in current EO studies, it is expensive and difficult to distribute to several accelerator positions. A fiber laser of appropriate wavelength and power will alleviate these difficulties.

There are two approaches we are pursuing. First, we will use an Er-doped fiber laser (1530 nm) which has already been purchased for time-of-arrival EOM measurements (see section 3.1.3), to investigate both spectral and spatial decoding techniques. One difficulty with this approach is that the group velocity mismatch inside the commonly used EO crystal (such as ZnTe or GaP) between the THz wave and 1530 nm is larger than the Ti:Sapphire case. This is a severe problem for measurements of very short bunches (<200 fs). This will not be an issue in our measurements of 200-2000 fs bunches. At the same time we will also investigate the possibility of using frequency doubling of the 1530 nm as our EO probe. Second we will construct in-house a fs fiber laser based on Yb-doped fiber (1030 nm). This wavelength would greatly reduce the mismatch caused by the longer wavelength Erbium laser. Figure 3.25 is a simulation of EO sampling for different laser wavelengths and shows that the change in measured bunch length is small for a 1 ps bunch. This indicates that EO sampling with fiber lasers is a viable option for the intermediate bunch lengths proposed at A0.

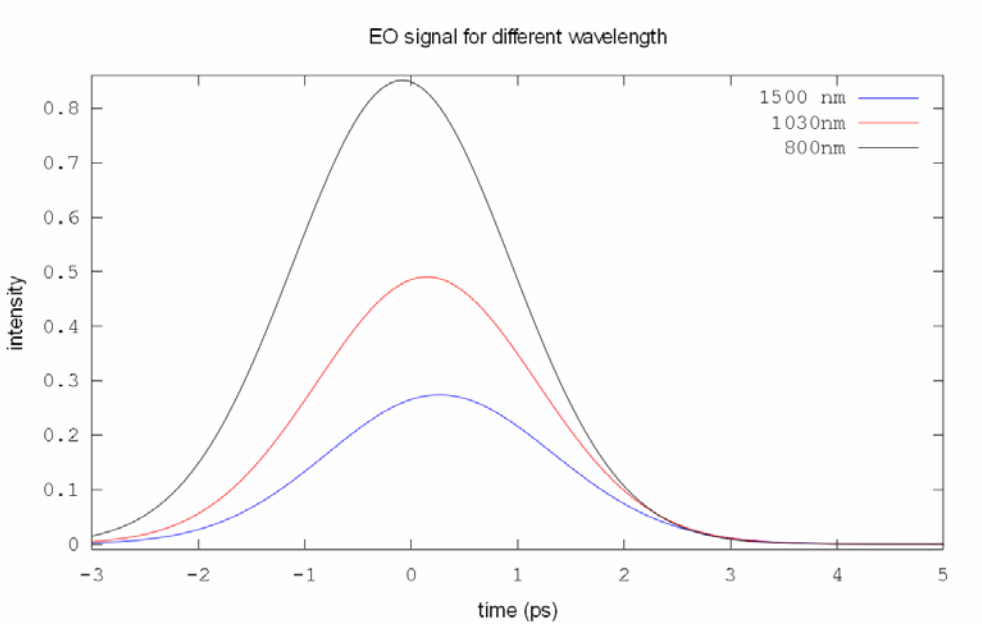

Figure 3.25: Simulated EO signal using 3 different laser wavelengths. Electron beam bunch length is 1 ps rms with a bunch charge of 1 nC. The EO sampling crystal is 1 mm thick ZnTe and 5 mm away from the beam center. Gaussian fits of these curves give rms values of 1.025 ps, 1.032 ps and 1.06 ps for 800 nm, 1030 nm and 1500nm respectively.

3.3 Other diagnostics

3.3.1 HOM signal processing

RF accelerating cavities can support, apart from the accelerating mode, a multitude of resonant modes, the so-called higher order modes (HOM). These modes are excited by the charged particle beams and can lead to an increase of the beam emittance or even to beam break-up in large accelerators. However, the HOMs can be useful for beam diagnostics. The dipole modes have a linear dependency of their amplitude and phase with the beam offset and angle. Therefore they can be used for position monitoring, similarly to cavity beam position monitors (BPM). By measuring the phase of monopole modes excited by the beam with respect to the injected fundamental mode, one obtains the phase of the beam relative to the RF. The monopole and dipole modes are shown in Figure 3.26.

Broadband HOM-based beam phase detection

The HOM couplers are not perfect and due allow some of the 1.3 GHz RF drive to pass through. This allows direct measurement of the phase of the monopole modes with respect to the 1.3 GHz RF. A simple test system has been implemented in the FLASH linac at DESY which simply digitizes a single HOM coupler signal with a fast 20 GS/s, 5 GHz bandwidth scope and then uses Fourier analysis to measure the relative phase. This system has demonstrated a 0.1° (@ 1.3 GHz) measurement RMS over a couple of hours and has reproduced requested phase changes to the drive RF. In principle this measurement can be improved by implementing dedicated electronics to split the HOM signal and downmix the fundamental and a selected monopole to a convenient IF (~20 MHz) and then digitize. This should greatly improve the signal to noise but does introduce potential phase shifts which need to be understood. This system is very useful to

monitor the phase of the RF system and could be used to provide slow feedback for phase stability.

Narrowband HOM-based BPM and cavity alignment observation

The dipole modes behave exactly like a cavity BPM with very high Q. The system implemented at FLASH uses analog downmix electronics to downmix electronics shown in Figure 3.27 to select a dipole mode which couples strongly to the beam. Tests at FLASH have demonstrated resolutions of less than 10 μm for a single bunch and the ability to provide bunch-by-bunch measurements for 1 MHz bunch trains. The system requires calibration by moving the beam through known trajectories in the cavity which is typically done with other BPMs. The narrowband system is very timing sensitive and requires good stability between the RF, LO, and trigger.

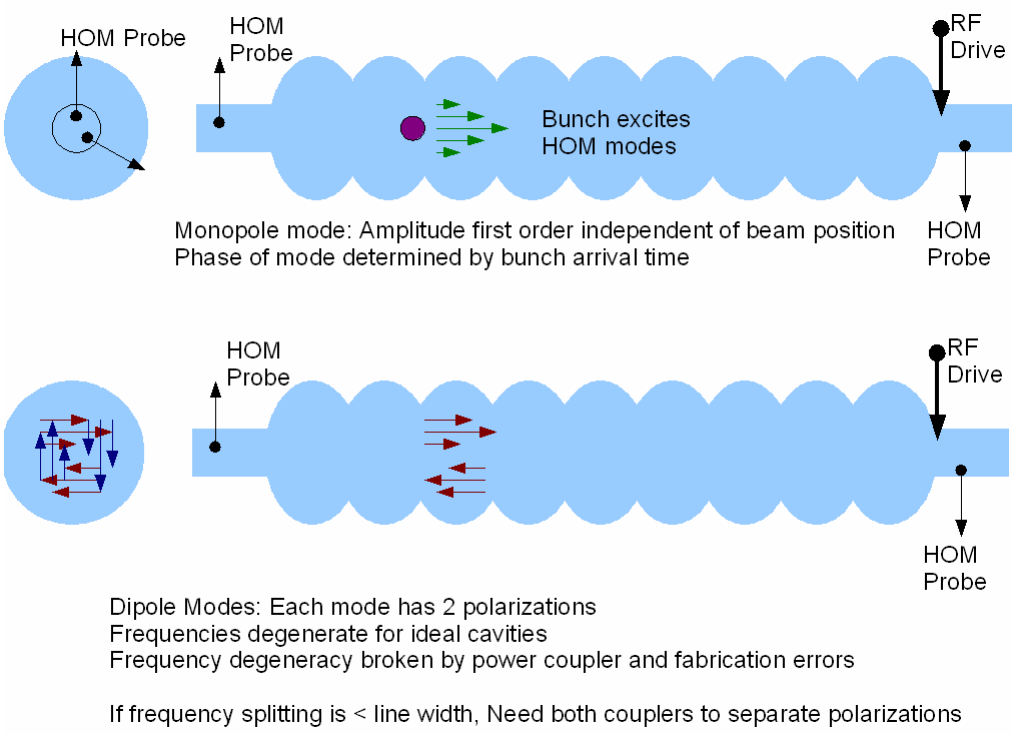

Figure 3.26: Monopole and dipole modes in a Tesla 9-cell cavity.

The HOMs can also be a useful tool for studying the superconducting cavities under operating conditions. The observed modes can be compared to predicted modes from simulations and test stand measurements. For this reason, a narrowband system capable of measuring different modes is very attractive. This makes implementing the LO, trigger, and downmix electronics challenging given the phase stability which is required.

Plans

In the current A0 accelerating cavity setup both HOM coupler signals are buried in the cryostat and are unfortunately not accessible. With a new or modified SCRF module these signals will be ported to the outside, allowing analysis of these HOM signals. We plan to investigate both techniques, broadband HOM signal analysis using our (to be upgraded) fast oscilloscope (12

GHz realtime BW), as well as a narrowband read-out system based on a 125 MSPS VME digitizer currently under development.

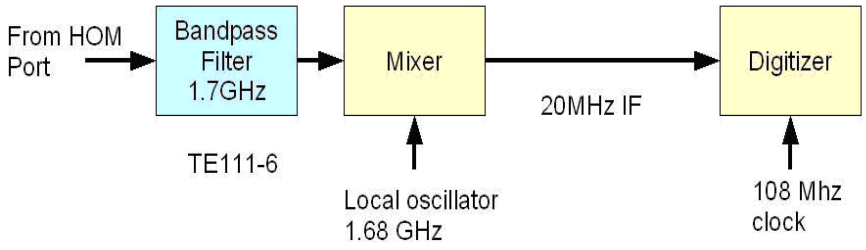

Figure 3.27: Narrowband downmix electronics scheme.

3.3.2 Cavity BPM

In frame of the ILC global design effort, a high resolution (0.5-1 μm) beam position monitor, based on a common-mode free L-Band cavity is under development for application in the SRF cryostat (quad-BPM package) (Figure 3.28). The manufacturing of a warm prototype is currently underway, it has dipole-mode read-out ports (f_{110}~1.5 GHz) for the displacement signals, as well as monopole-mode ports (f_{010}~1.1 GHz) for beam intensity normalization. The loaded Q is Q_l~500-700, which allows single bunch beam position measurements (>300 ns bunch-to-bunch spacing). After tuning and characterization on an RF test stand, we are planning to analyze the cavity BPM in detail under realistic beam conditions at the A0 Photoinjector. It is necessary to understand how well the tuning suppresses the x-y coupling, CM rejection in the dipole mode signals, single bunch behavior, signal processing, noise figures, etc. to fully characterize resolution and dynamic range under real world conditions.

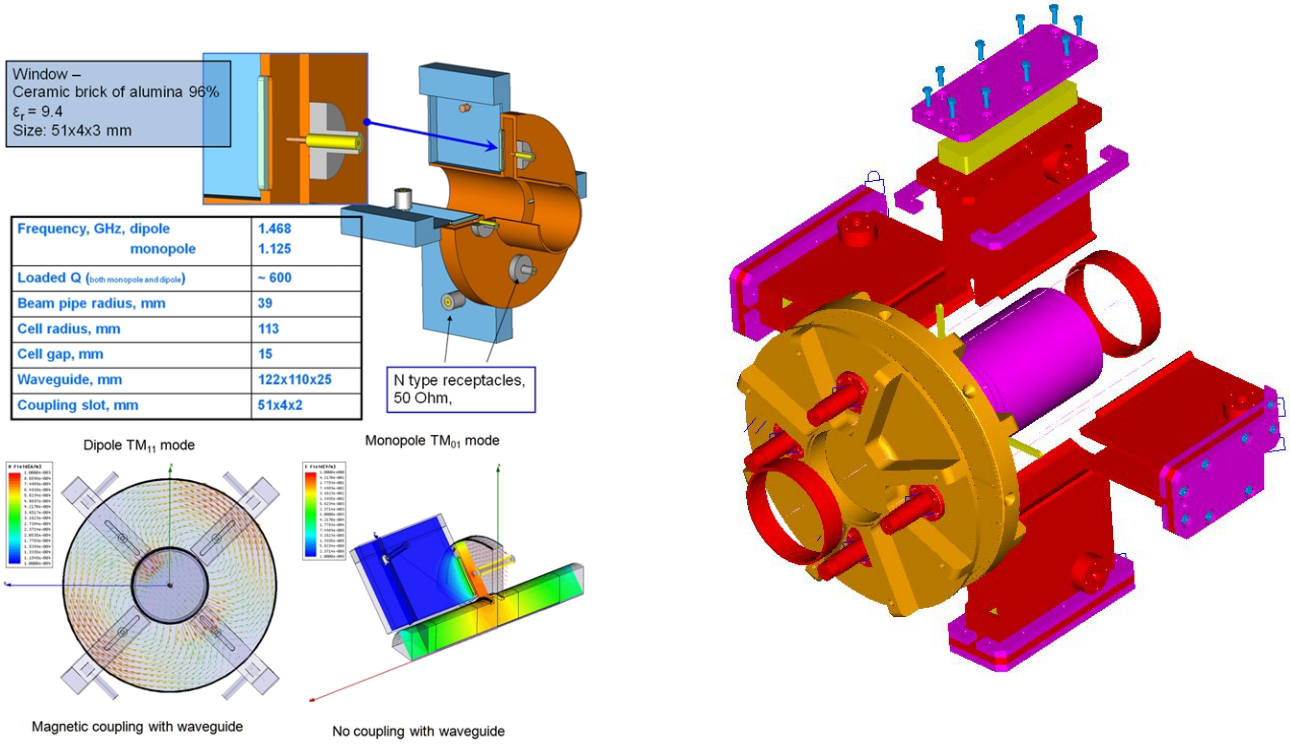

Figure 3.28: CM-free L-Band cavity BPM for the SRF cryostat.

3.3.3 Waveguide pickup

We propose this technique, as it is a quite simple and inexpensive technique to estimate the bunch length and verify the bunch compression.

The frequency domain magnitude spectrum of the beam is observed at a radiating ceramic gap at several (2-4) frequencies. Horn-antennas, waveguides, and detector elements are commercially available in a range 90-900 GHz. Similar experiments were executed at the SLAC Endstation-A and at the CERN CLIC Test Facility (Figure 3.29). The response time of the detector elements is <<1 ns and the noise characteristics are excellent, thus allowing single bunch measurements. The setup is very simple and straightforward, however an absolute calibration of the bunch length is extremely difficult (no phase information, unknown insertion loss, and unknown sensitivity among the different frequency channels). However, this simple, inexpensive method gives a non-invasive, relative observation of the length of each single bunch.

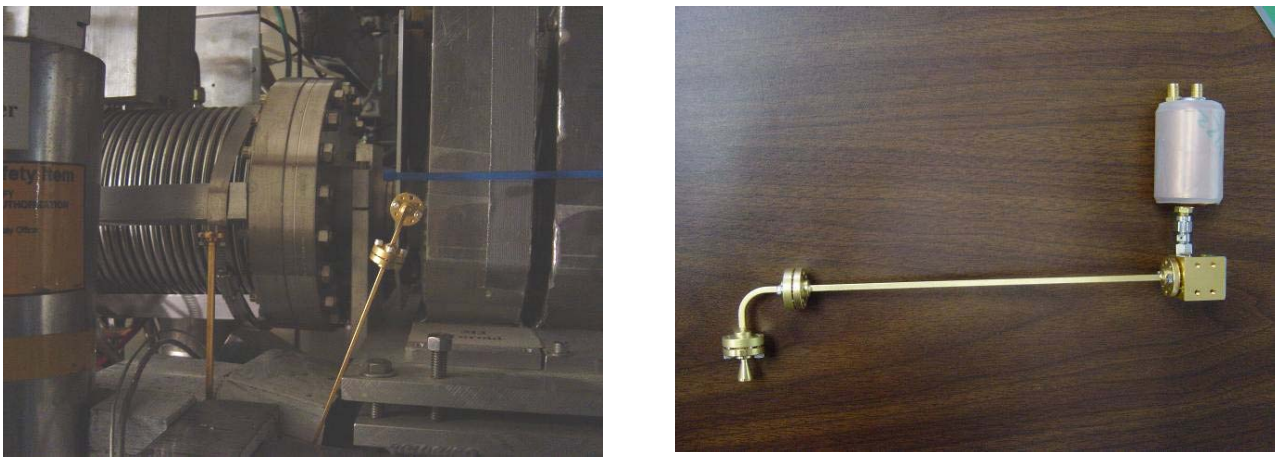

Figure 3.29: 300 GHz waveguide pickup system tested at SLAC ESA.

References

[1] J. Corbett *et al.*, in *Proc. PAC2007, Albuquerque, NM*, FRPMS065, p. 4159.

[2] A. Lumpkin, J. Ruan, "Initial Synchroscan Streak Camera Imaging at the A0 Photoinjector", submitted to *Proc. BIW2008, Lake Tahoe, CA*, (to be published).

[3] F. Loehl, THOBF101, in *Proc. EPAC2006, Edinburgh, Scotland*.

[4] F. Loehl, WG506, in *Proc. Future Light Source 2006, Hamburg, Germany*.

[5] A.G. Shkvarunets, R. B. Fiorito, Phys. Rev. ST Accel. Beams **11**, 012801 (2008).

[6] A. G. Shkvarunets, *et al.*, in *Proc. DIPAC2007, Venice, Italy*.

[7] G. Berden, *et al.*, Phys. Rev. Lett. **99**, 164801 (2007).

[8] S. P. Jamison, *et al.*, TUYPA01, in *Proc. EPAC2006, Edinburgh, Scotland* .

[9] A. L. Cavalieri, *et al.*, Phys. Rev. Lett. **94**. 114801 (2005).

4 Facility upgrades

4.1 Overview of upgrades

The gun and cathode chamber will be replaced by newer versions from DESY and INFN Milano, respectively. The new cathode chamber will allow for easier changing of the cathodes and the ability to prepare cathodes outside of the beamline cave. The new gun with its on-axis coaxial input coupler will improve gun operation, increase beam energy, and reduce dark current, breakdown, and emittance.

The current beam energy of 16 MeV is relatively low and space charge effects still play a significant role in the beam dynamics. Increasing the beam energy to ~30 MeV would reduce space charge effects by a factor ~4 and increase the stiffness of the beam. We are currently considering two options. A first option [option (1)] is to replace the present SRF cavity with an existing cavity with a gradient of >25 MeV. This cavity and cryomodule has already been assembled and commissioned at Fermilab [1]. However, the high gradient in this cavity just downstream of the gun may over-focus the beam. For these reasons we also are considering the use of two SRF cavities [option (2)]. The first cavity downstream of the RF gun would be operated to medium gradient ~15 MV/m, while the second cavity would be operated at its maximum gradient. This latter solution offers more flexibility. For instance the compression in the downstream chicane could be controlled by the phase of the second cavity while for the single cavity scenario, operating the high gradient cavity too far off-crest would result in unavoidable longitudinal compression via velocity bunching. However, an accelerator configuration including two SRF cavities would probably require an extension of the beam enclosure outside the current building. These options need further evaluations and in the following we consider both options. Preliminary simulations indicate that option (1) is viable (see Figure 4.1). Reasonable transverse beam emittance are achievable at ~30 MeV with a single accelerating cavity.

The accelerating cavity(ies) are followed by a round-to-flat beam transformer composed of three quadrupoles, a set of normal quadrupoles, and is then split into two lines. One line will have a vertical chicane with straight through capability, and the other line will have the double dogleg configuration. Both lines will have spectrometer dumps.

As bunch length measurements will become a primary focus, we will require a reliable diagnostic by which to benchmark other diagnostics begin developed. To date, deflecting mode cavities used to streak the beam are capable of the best time resolution. At Fermilab R&D has already taken place on the development of a superconducting deflecting mode cavity, and the RF power source for such a cavity exists. At the end of each beamline some meters before the spectrometers, space will be allocated for the superconducting deflecting mode cavity. At this time only one is planned for installation but the cryogenics will be arranged so that it can feed the cavity in either location.

Space will be available for experimental setups such as an image charge undulator or an inverse Compton scattering laser cavity. Figures of the present layout and the two options are shown in Appendix 7.2.

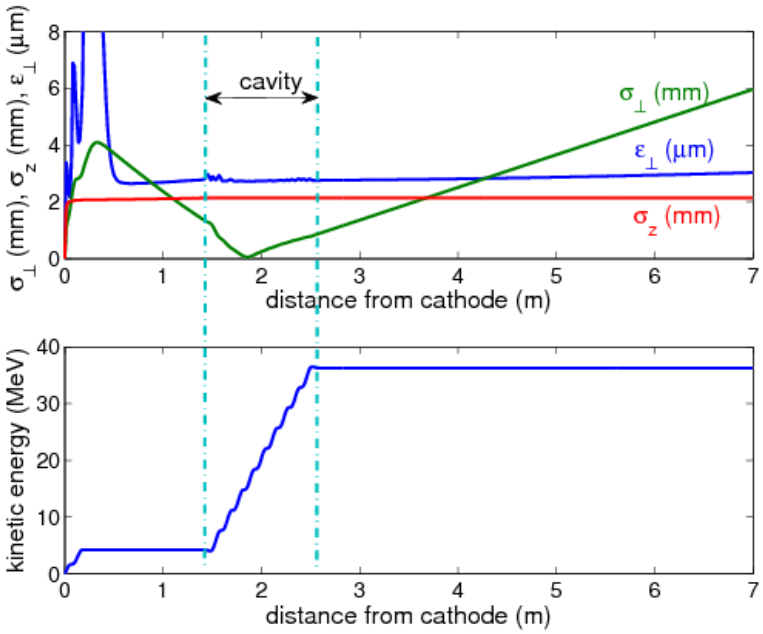

Figure 4.1: Beam parameters evolution for option (1) [see text for details]. Beam transverse rms size, emittance and bunch length (top) and kinetic energy (bottom) evolution along a possible option for the A0 beamline upgrade [option (1)]. The gun is assumed to be operated at 40 MV/m peak E-field and the charge per bunch is 1 nC.

4.2 RF gun

In conjunction with the TESLA collaboration, Fermilab has constructed and operated several L-band (1.3 GHz) photo-cathode RF guns. One of these guns is presently installed at the A0 photoinjector, while another gun was installed at the DESY TTF. Both these Fermilab-built guns have exhibited deficiencies: namely, RF break-downs at long pulses caused by excessive heating at the input coupler slot. Dark current has also been an issue but this is more likely a feature of the cathode than of the gun. The gun at DESY TTF was later upgraded with a new RF gun, while the Fermilab gun has remained in operation. Fermilab has recently obtained all documentation needed to produce this new upgraded RF gun. This DESY-type RF gun will be procured, commissioned and installed at A0 as part of the upgrade. It is schematically shown in Figure 4.2. The DESY-type gun has been characterized at DESY Zeuthen PITZ [2] where they measured normalized 90% emittances of ~1.5 mm-mrad at 1 nC. The normalized 90% emittance measured at the end of the 120 MeV injector at DESY is ~2 - 2.5 mm-mrad with 3MW gun rf power. These measurements give us some expectation that we may improve our beam emittance after the new gun and capture cavity are installed to provide 30 MeV beam. RF power for the gun will remain the same as at present (3 MW) and limit the gradient on the cathode to about 30 MV/m. Table 4.1 summarizes the main parameters of the RF gun.

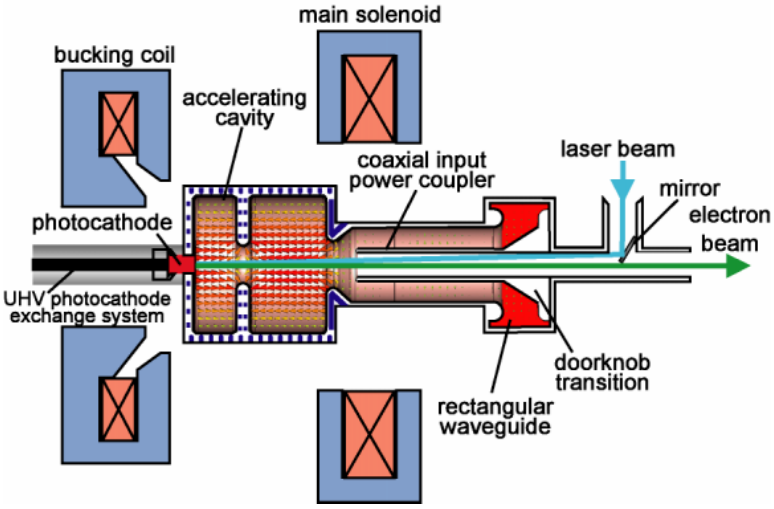

Figure 4.2: Schematic of the DESY-type RF photo gun.

Table 4.1: The main RF gun parameters

electrons/bunch	2×10^{10}
bunches/pulse	up to 3000
bunch repetition rate	3 MHz
pulse repetition rate	up to 5 Hz
average current	50 μA
beam energy	4.5 MeV
RMS bunch length	1 – 6 mm
RMS normalized emittance	4-5 μm

The difference in design between the Fermilab and the DESY guns will require the following other components to be replaced at the A0 photoinjector: (1) the gun cavity itself, (2) the focusing solenoids, (3) the coaxial RF coupler, (4) the laser mirror cross, and (5) the cathode exchange system.

The current drive laser system can deliver a 300 flat-top pulse train with an energy of 5-10 μJ per UV pulse on the photocathode surface. However, further improvements remain to be addressed. The current laser system is not able to deliver a flat pulse train over 1 ms that can meet ILC requirements. Though long pulse trains will not be required at A0, we will continue development already started on providing long flat pulse trains. The source of these deficiencies is the Nd:Glass gain medium used inside the multi-pass cavity. In addition, the pulse picker that selects individual oscillator pulses for amplification does not cleanly reject adjacent pulses.

We have recently developed a diode laser pumped Nd:YLF multi-pass system. Initial tests demonstrate that it can deliver a long flat laser pulse train (1000 pulses @1 μs/pulse). This multi-pass amplifier will replace the current multi-pass cavity which is based on Nd:glass pumped by the flash pump. We will eliminate the extraneous pulse by adding an additional pulse picker between the multi-pass structure and 2-pass structure.

4.3 SRF acceleration cavities

As outlined in the introduction, we consider two upgrade scenarios.

Replace the single SRF accelerating cavity with a higher gradient SRF cavity

We plan to replace the present TESLA accelerating cavity (CC1) that follows the gun with a higher gradient cavity currently under test at the Meson Lab Test Facility. This cavity has achieved a gradient of ~25 MeV/m, so we expect a beam energy of ~30 MeV at its output. This cavity is mounted in a similar cryomodule as is currently in use at A0. The cavity module will have to be moved slightly downstream in the A0 cave because of the longer length of the DESY gun assembly. This will require relocation of the cryogen feed line.

Add a 2nd SRF accelerating cavity

In this case we will make minor repairs to the CC1 module, relocate as above, and install the 2nd SRF cavity behind it. This will require two cryogen feeds and an additional 300 kW RF system. With this arrangement the cave will be extended by about 3 meters.

4.4 Additional deflecting mode cavity

Deflecting mode cavities provide a method of measuring the longitudinal bunch distribution and have been used for many years at SLAC and DESY for this purpose[3][4]. The method relies on the transverse kick as a function of beam arrival time in the deflecting cavity. This kick maps the bunch length into the deflecting plane. If the beam is imaged at a suitable location downstream of the deflecting cavity then the longitudinal bunch profile can be determined.

At the A0 Photoinjector a streak camera is currently used to measure bunch lengths, and it has a single bunch resolution of ~1.5 ps rms. At bunch lengths shorter than 1 ps, a Martin-Puplett interferometer is used, but this method requires multiple bunches per train and many minutes of data taking to obtain an accurate measurement. The analysis relies on certain assumptions of the bunch shape and frequency response of the detector in order to reconstruct the shape of the bunch and also loses information about the head tail orientation of the bunch.

We wish to improve our method of measuring the short bunch lengths by using a stronger deflecting mode cavity. Our goal is to have a system that can measure the bunch length of a single bunch with a resolution ~300 fs rms over the entire range of bunch lengths available at A0, and with none of the disadvantages of the interferometer.

Currently at the A0 Photoinjector there is a 3.9 GHz 5-cell copper cavity based on a superconducting deflecting cavity designed for a separated kaon beam experiment. This cavity is cooled with liquid nitrogen to increase the Q and separate the modes. It is powered by an 80 kW klystron, and the integrated deflecting field is 550 kV. It is currently used for the emittance exchange experiment at A0. It does not have sufficient voltage for measuring bunch length with the required accuracy. A superconducting cavity constructed with 9 cells will provide approximately 2.0 - 2.5 MV integrated deflecting field.

Figure 4.3 shows the beamline with a matching section prior to the cavity, the deflecting cavity, a drift length and a flag to image the beam. The purpose of the matching section is to focus the beam at the flag when the cavity is turned off. This will provide the greatest resolution. We shall assume that the beam can be focused to a 0.1 mm rms spot at the flag, and the flag is located 1 m downstream of the deflecting cavity.

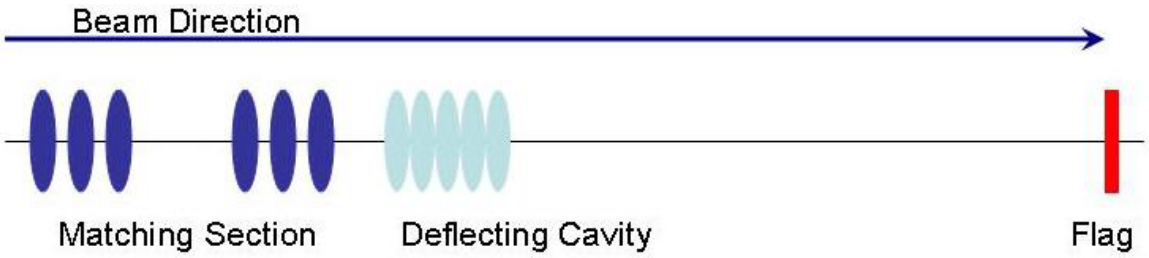

Figure 4.3: Schematic drawing of a bunch length measurement using a deflecting cavity.

The deflecting cavity is operated at the zero crossing of the deflecting field which will give no net deflection to the bunch, and kick the head and tail in opposite directions. The beam spot at the flag, with the deflecting cavity on, is then

$$\sigma_{x-flag}^2 = \sigma_{x-cavoff}^2 + \sigma_z^2 k^2 \left(L + \frac{L_c}{2}\right)^2$$

where $\sigma_{x\text{-flag}}$ is the beam spot at the flag location, $\sigma_{x\text{-cavoff}}$ is the beam spot at the flag when the cavity is turned off, σ_z is the bunch length at the deflecting cavity, L_c is the deflecting cavity length, and L is the drift length from the downstream end of the cavity to the flag. k is given by

$$k = \frac{eV\omega}{Ec},$$

where eV is the integrated transverse kick, c is the speed of light, ω is the angular frequency and beam energy is E. For the 9-cell superconducting cavity, k=7 m^{-1} at 30 MeV, and 15 m^{-1} at 15 MeV. For comparison, the 5-cell copper cavity has 3 m^{-1} at 15 MeV.

Assuming the drift length is 1 m and the imaging system for the flag is identical to the current system, Figure 4.4 shows the inferred bunch length vs. the actual bunch length for the proposed system at 30 MeV beam energy. The smallest bunch length that can be measured is 50 fs rms.

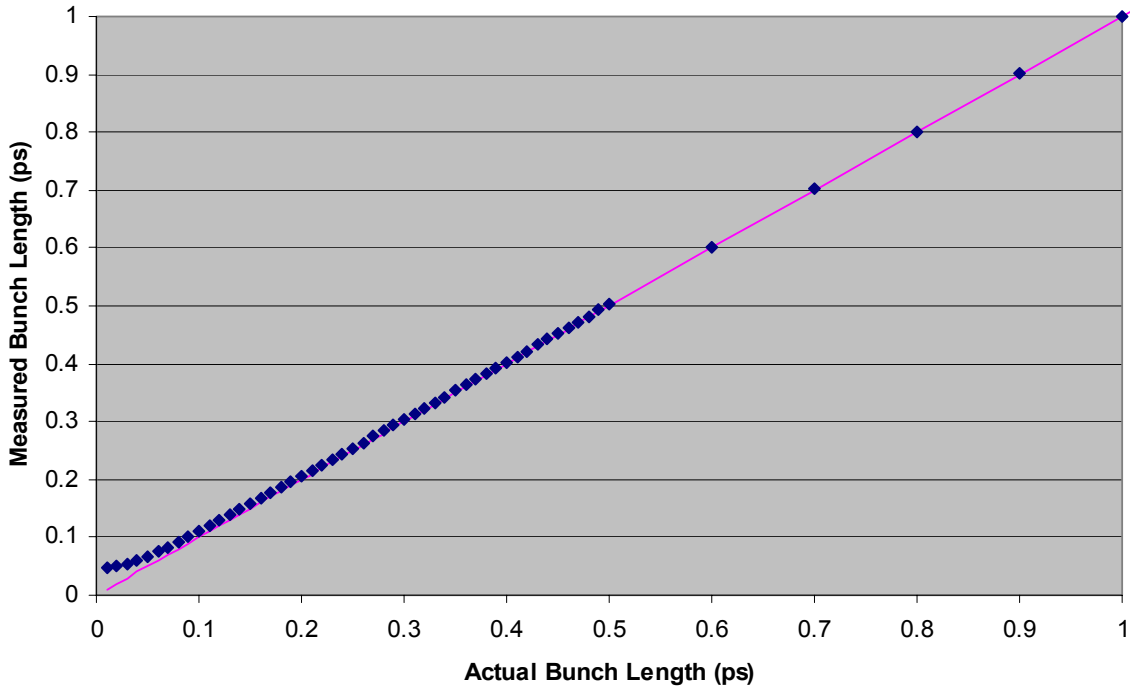

Figure 4.4: The measured bunch length vs. the actual bunch length. Blue dots are the measured length. Pink line is actual length. The minimum resolvable length for a single bunch is 50 fs.

Over the years considerable development work has been done on the design of a deflecting mode cavity. Prototypes have been built and a 3-cell cavity tested in a vertical dewar. It achieved 7.5 MeV/m deflecting gradient (Figure 4.5).

At A0 all the cavity ancillaries will use the designs developed for the 3.9 GHz accelerating mode "3rd harmonic cavities". These include input coupler, HOM coupler designs, helium vessel, and tuner. Outstanding design issues are associated with the lower order mode (LOM) and other polarization mode damping. These will be the real R&D developments for this design and are related to future applications such as crab cavities for the ILC interaction region. For the application at A0 we will be running short bunch trains and mode damping will not be that much of an issue. Even so, this is an opportunity to try various LOM designs.

The cryogen insulating vacuum module will be designed to accommodate one 9-cell cavity of either accelerating or deflecting verity. It will interface to the standard cryogen feed "top hat" design used both at A0 and in the Meson Lab SRF test areas. The length and diameter of the vessel will be ~ 1.1 m and 0.5 m, respectively.

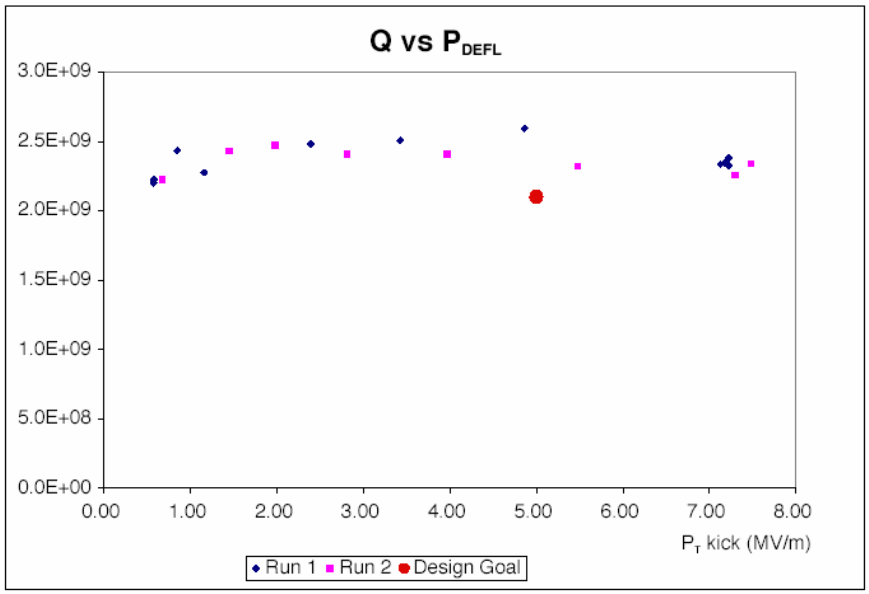

Figure 4.5: Results from a 3-cell TM110 deflecting mode cavity. Large red dot is design value; pink and blue dots are measurements. 7.5 MV/m corresponds to 120 mT maximum surface field.

4.5 Other components

Cryogenic System

The present 2K system at A0 is dewar fed with transfer lines to both the photoinjector area and the "north cave" area where vertical dewar tests are preformed. Vacuum pumps provide the pumping for the 2K and the boil off helium gas is returned to the Fermilab Central Helium Liquifier where it is recycled. Usage at present is about one 500 liter dewar per day. In addition, the emittance exchange deflecting mode cavity is cooled by LN_2.

Modifications will have to be made to support additional SRF cavities -- one 3.9 GHz deflecting mode cavity and possibly an additional 1.3 GHz accelerating mode cavity. The modifications consist mainly of relocation of existing feed and vacuum lines for the different CC1 location (and possible additional CC2) and new lines and feed hat for the 3.9 deflecting mode cavity. It is expected that the dewar usage will double and the 2K vacuum pumps will need to be supplemented.

High Level RF system

The RF systems at A0 presently consist of 1) the 1.3 GHz 3-4 MW gun system; 2) the 1.3 GHz 250 kW SRF CC1 system; and 3) the 3.9 GHz 80 kW emittance exchange nitrogen-cooled cavity system. These can run for beam pulse lengths of 0.5 to 1 ms at 1 Hz.

The proposed 3.9 GHz deflecting mode cavity will use a small existing 4 kW klystron power system. A second "CC2" accelerating cavity would require an additional 250 kW system. Such a system has been assembled at NML and will be used to test CC2 there later this year. It could then be moved to A0. The gradient of the emittance exchange cavity can be doubled with the addition of another 60 kW RF klystron. This will provide enough gradient to operate at 30 MeV beam energy.

Low Level RF system

The present LLRF system coordinates and regulates the timing, RF phases and amplitudes of the three RF cavities and the laser. This system will be enlarged for two more cavity systems. The systems are state-of-the-art FPGA-based regulation systems for each cavity. The approach is based on the developments at the DESY FLASH and XFEL facilities. Additional R&D and improvements to the system and controls interface are being implemented at Fermilab.

A0 provides a unique test bed for this ongoing development and improvement program as it is the only place at Fermilab where the systems and feedback algorithms can be rigorously tested with beam, as an integrated multi-cavity system.

Controls

The control and data acquisition system for the A0 Photoinjector is based on the DOOCS (Distributed Object Oriented Control System) package from DESY. This package includes a framework for writing front-ends in C++ and a client for creating and displaying virtual control panels for operators. This client (DDD) is a C++ application based on the XView windowing toolkit and currently unsupportable. It is difficult to work with and maintain, and the XView toolkit is out-of-date.

A replacement (jDDD) is in active development at DESY and shows promise. It is a complete rewrite of DDD in modern Java. Unlike DDD it is consistent with current GUI conventions making it much easier to learn and use. There are a number of small bugs and missing features which must be addressed before it can be used for operations. We plan to work with DESY in correcting these and other issues while testing jDDD.

Beam Monitor Read-out Systems

The read-out electronics systems for most basic beam monitors (e.g., toroids and beam position monitors) are outdated or temporary installations, unable to deliver the required performance and reproducibility of the beam parameters to be characterized. A new, low-cost 100 MS/s 8-channel VME digitizer, recently developed in-house, will replace old analog signal processing installations for beam position and intensity measurements. The BPMs will be equipped with a downconverter/calibration unit, already successfully tested at the ATF damping ring at KEK.

Beam line components, magnets, and power supplies

New beamline components will need to be assembled, although most of the existing components will be reused. These components will be similar to those installed for the emittance exchange experiment and include: vacuum pipe, pumps, gate valves, gauges, diagnostic crosses. Some new magnets and power supplies may be necessary to handle the higher energy.

Radiation & Shielding

The radiation limit outside the cave is set to 1 mrem/hr and on the roof of the cave to 5 mrem/h. At the present 16 MeV operating energy an administrative beam current limit of 300 nC/sec applies. The existing enclosure shielding thickness is 320 gm/cm^2. At the higher energy of 40 MeV, we will have to determine the allowable pulse length and bunch charge to stay within the above limits. The increased neutron yield is the primary worry. Previous calculations for our geometry give 0.6 mrem/h for neutrons produced from a copper dump at 0.3 μA beam current at 50 MeV. For x-rays and gammas produced in the beam dumps, present shielding should be sufficient. For losses outside the dump, some areas may need to be locally shielded or losses

kept to ~<10%. As a reference, an early estimate based on an average current of 4 μA at 50 MeV required an additional 30 cm of shielding. If necessary this could be added outside the cave structure. There are some weak spots in the present shielding, e.g. where the ventilation air enters. These weak spots will be addressed during the upgrade.

Extension of the Cave

In the case in which two 1.3 GHz SRF cavities are installed, the cave will have to be extended by about 3 m. This can be achieved by building a shielding block extension outside the building at the south end. Presently there is a gas bottle shed in the area that would be relocated.

4.6 Connections to other technologies

SRF R&D

The A0 building supports an ongoing SRF research area with clean room, clean assembly area, high pressure rinse system and vertical dewar testing. Continued research and testing is planned for the area and the A0 technicians support both this activity and the A0 photoinjector operations. The A0 area is the ideal place to test small special research cavities such as special coatings, single crystal special cavities, alternative processing, etc. Tests of both 1.3 and 3.9 GHz cavities takes place here.

Polarized electron gun and cathode chamber, SRF gun.

Our long term vision is to provide an ILC quality like beam to the linac without having to build a damping ring. This concept has been extant not only at Fermilab but at other labs as well for a number of years now. It is directly related to the various emittance studies and manipulations we are carrying out: the round-to-flat beam transformation, the emittance exchange experiment, and the ring beam adiabatic capture process.

An RF gun that will support the use of GaAs cathodes needs to be developed. Such a gun could be a room temperature gun with a very good vacuum or an SRF gun. There are ongoing developments in both areas. We would like to be part of these developments but have so far been limited by resources. The development of a SRF gun with a GaAs cathode and magnetic field on the cathode to provide for flat beam development would be a goal. As others are working on this technology challenge we would need to collaborate closely with them. We are also willing to aid in SBIR work focused toward other types of guns that might support the GaAs cathodes. We currently have a cathode chamber provided from AES for studying the GaAs cathodes and their lifetimes. However so far we have made little progress in this direction because of other priorities and limited resources.

4.7 Collaborations and students

The A0 Photoinjector has an extensive history of collaboration with other groups and institutions. Much of the hardware that makes up the photoinjector has come from other groups, and people from other institutions have spearheaded or been involved with both the specific projects and the hardware or equipment that make up the photoinjector. These collaborative activities are summarized in Table 4.2.

At present Argonne, Northern Illinois University, Fermilab, and University of Chicago are collaborating in a partnership-like arrangement where we try to supplement each others activities and build on the interchange of both ideas and utilization of equipment and resources. We are

hoping to enlarge this group to include participation from others such as University of Maryland, University of Wisconsin, and MIT. At present, discussions of possible mutual interest are only in initial phases. We believe we have a facility that well complements that at Maryland and student studies of photoinjector issues and diagnostic development of short bunches could complement their activities. Both Wisconsin and MIT are interested in SRF injector development as well as in electron laser interactions.

Collaboration continues with DESY and INFN Milano on RF gun development.

Table 4.2: Collaborating and participating institutions, past and present.

institution	equipment	projects/people
Argonne		emittance exchange, EOS
Cornell	4 MW klystron, SRF equipment	ILC fast kicker and tests
DESY	TESLA SRF cavities CC1 and CC2, 300 kW klystrons, RF guns, LLRF, DOOCS controls, Martin-Puplett interferometer	Flat beam
Fermilab		all
LBNL		Flat beam
INFN Frascati	intensified camera (loan)	student and use of camera
INFN Milano	cathode preparation chambers	commissioning of cathode systems
NIU	helium gas recovery system, laser oscillator	electro-optical imaging
Rutgers		emittance exchange, CC2 install and test
Saclay/Orsay	SRF cavity cryostats, tuner	injector characterization
UCLA	plasma chamber, magnets	plasma wakefield acceleration and focusing, photoinjector design
Univ. of Chicago		Flat beam
Univ. of Illinois		ILC fast kicker, students and tests
Univ. of Rochester	drive gun laser and additional equipment	Laser assembly, commissioning, EOS, laser acceleration, two macrobunch compression

Students and their supervision are a specific issue for the A0 photoinjector. A list of past and present students is given in Table 4.3. For the activities at A0 to be effective there must be a critical mass including both staff and students. We must find stable student sources in order to have a viable program. In the past many of the students have come from University of Rochester and UCLA. We look forward to students from NIU and Chicago, but we must establish other strong university connections.

Table 4.3: Past and current graduate students at A0 photoinjector

name	institution	date of PhD	thesis topic	current institution
Eric Colby	UCLA	1997	RF photoinjector gun	SLAC
Alan Fry	Univ. of Rochester	1998	laser development	
Mike Fitch	Univ. of Rochester	2000	electro-optical sampling	
Jean-Paul Carneiro	Universite Paris XI	2001	experimental studies of photoinjector	Fermilab
Yin-e Sun	Univ. of Chicago	2005	flat beam transform	Fermilab
Rodion Tikhoplav	Univ. of Rochester	2006	laser acceleration	UCLA
Tim Koeth	Rutgers Univ.	current	emittance exchange	
Artur Paytyan	Yerevan Univ.	current	SC RF controls	
Timothy Maxwell	NIU	current	EO imaging	

References

[1] T. Koeth *et al.*, in *Proc.PAC2007, Albuquerque, NM*, p. 2251.

[2] Phys. Rev. ST Accel. Beams **9**, 092802 (2006); WEPPH008, in *Proc. FEL2007, Novosibirsk, Russia*.

[3] R. Akre *et al.*, in *Proc. PAC2001, Chicago, IL*, p. 2353; R. Akre et al, Phys. Rev. ST Accel. Beams **11**, 030703 (2008).

[4] B. Beutner, Ph.D Thesis, University of Hamburg (2007).

5 Transition to Mid-West AARD Center (NML)

The Tesla Test Facility at DESY has provided a valuable system test for many elements of the TESLA SRF technology. However, several important changes to the TESLA RF cavity and cryomodule design are being planned for the ILC and for the Project X at Fermilab. These will include a higher cavity gradient, relocation of the quad, shortening of the cavity end-group, and a new tuner design. Such changes will likely be introduced in several steps, with the first one being called a Type-IV cryomodule design. Also under discussion are different modulators, klystrons, cavity shapes, and other things. The minimum size system test needed to confirm the performance of such a new design is a single RF unit (3 cryomodules) with an ILC-like beam. As many tests are statistical in nature, a larger test or multiple tests might be required.

Presently, Fermilab is building an ILC RF unit test facility, called NML, at the existing New Muon Lab building. The NML will be the only U.S. facility capable of testing completed cryomodules. The facility will be capable of testing cryomodules at high accelerating gradients with an ILC-like beam. The NML will perform the initial tests of Type-IV cryomodules. The goal is to produce a single RF unit (two Type-III+ and one Type-IV cryomodules) by the end of FY11, and a complete RF unit, made up of Type IV (or higher) cryomodules, by about a year later. This facility will be invaluable to the SRF R&D program leading up to and most likely through the Project X construction. It will allow for a dedicated study of dark currents, HOM extraction, alignment, LLRF and control issues, cryogenic issues, RF power distribution, reliability and system recovery issues. Although the SRF program will be the first user of this facility, it will not be the only user. As the need for SRF-related tests diminishes, the facility will start serving other users, such as the Advanced Accelerator R&D projects and experiments.

The NML RF unit test facility will consist of (1) the electron injector area (approximately 15 m long), (2) the accelerator area, comprised of 1 or more cryomodules (approximately 40 m) and (3) the test beam lines area. The existing New Muon building will accommodate such a layout, however the AARD needs will require the building to be extended in order to accommodate additional test areas. Initially, a temporary cryogenics system will be installed in the building. A new cryogenics plant will be added to the facility in the future in order to accommodate the correct fluid temperatures and to provide higher cryogenic capacities.

We assume the NML building will be extended or that the cryomodule string will consist of at most 2 modules allowing for space for an AARD program. Experimental areas could be provided at 25 – 50 MeV beam energy and also as high as ~750 MeV (with the RF cryomodules installed). In this case many of the experiments proposed here can be continued at NML. In addition, the following experiments have been discussed:

- ILC crab cavity tests
- Optical stochastic cooling
- in-vacuum laser acceleration
- beam driven acceleration in slab dielectric structures
- development of optical diffractive radiation diagnostics.

6 Schedule and required resources

6.1 Schedule

[editor's note: under development]

6.2 Resources

6.2.1 Summary of M&S cost estimates

[editor's note: under development]

6.2.2 Summary of labor estimates

[editor's note: under development]

7 Appendices

7.1 Parameters

Table 7.1: Current A0 photoinjector beam parameters

parameter	units	value
gun gradient @ cathode	MV/m	35-40
9-cell cavity accelerating gradient	MV/m	12
bunch spacing	μs	1
# of bunches/pulse		10 - 200
RF pulse length	μs	30 - 300
pulse repetition rate	Hz	1
cathode efficiency	%	0.5 -2.0
laser UV energy	μJ/bunch	16
FWHM laser pulse length, unstacked/stacked	ps	5/21
bunch charge	nC	1 - 10 typ.
kinetic energy after gun	MeV	4.0
kinetic energy after 9-cell cavity	MeV	16
gun solenoid peak field	Gauss	1200
laser spot radius @ cathode	mm	0.7 - 1.6
RMS normalized emittance @ 1 nC	10^{-6}m	4-6
RMS normalized emittance @ 8 nC	10^{-6}m	12.6
uncompressed beam		
RMS momentum spread @ 16 MeV @ 1 nC	%	0.25 - 0.38
RMS bunch length @ 1 nC	mm	1.6
RMS bunch length @ 8 nC	mm	2.9
peak bunch current	A	75 - 330
bunch compressor		
Compressor R56	cm	8
Compressor Max. Dispersion	cm	14
Compression Phase	degrees off crest	-39
Chirped Energy spread	%	1.32
Compressed Bunch Length @ 1nC	mm	0.21
peak bunch current	A	1400
double dogleg compressor		
Compressor R56	cm	24
Compressor Max. Dispersion	cm	66
Compression Phase	degrees off crest	-20
Compressed Bunch Length @ 1nC	mm	0.19
peak bunch current	A	1570
emittance exchange		
CC1 Phase	degrees off crest	-20
Beam Energy	MeV	14.3
Energy Spread	%	0.8
Bunch Length	mm	0.45

Table 7.2 Current A0 photoinjector drive laser parameters

parameter	units	value
oscillator frequency	MHz	81.25
oscillator wavelength	nm	1054
oscillator energy/pulse	nJ	5.5
energy/pulse after multi-pass	μJ	6
energy/pulse after two-pass	μJ	100
UV energy/pulse after crystals	μJ	20
UV energy/pulse on cathode	μJ	10
UV pulse length (FWHM)	ps	5
pulse separation	μs	1
length of pulse train		up to 800 bunches
train repetition rate	Hz	1

7.2 Facility layout

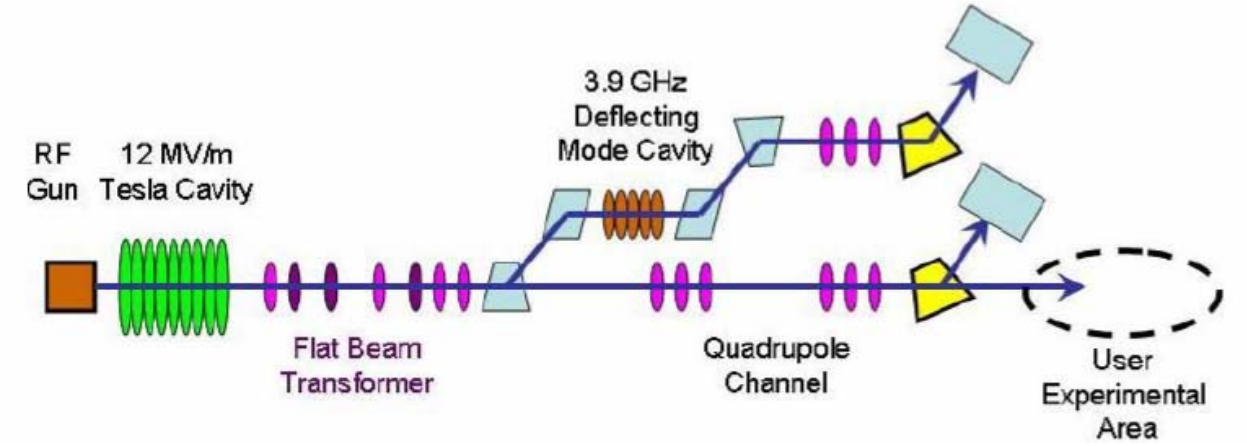

Figure 7.1: Current A0 photoinjector layout.

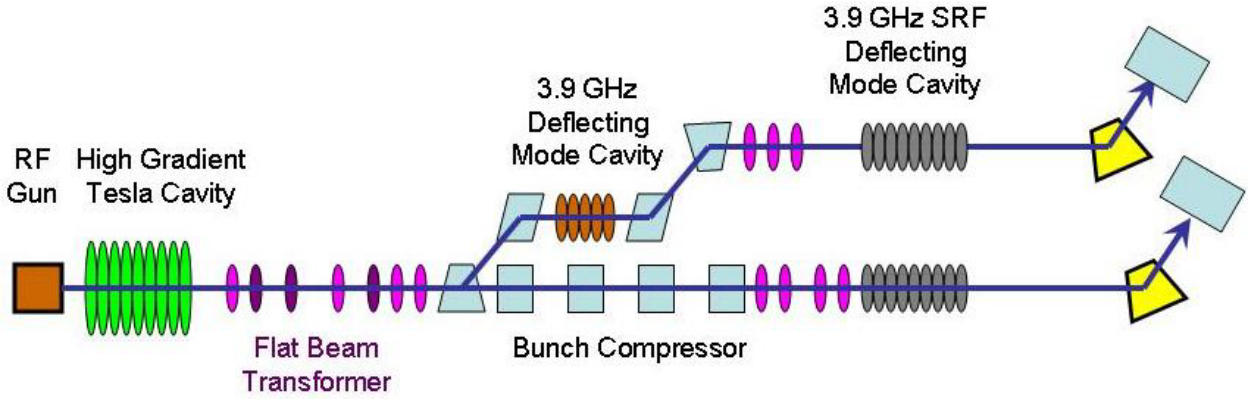

Figure 7.2: A0 Upgrade showing a single high gradient accelerating cavity.

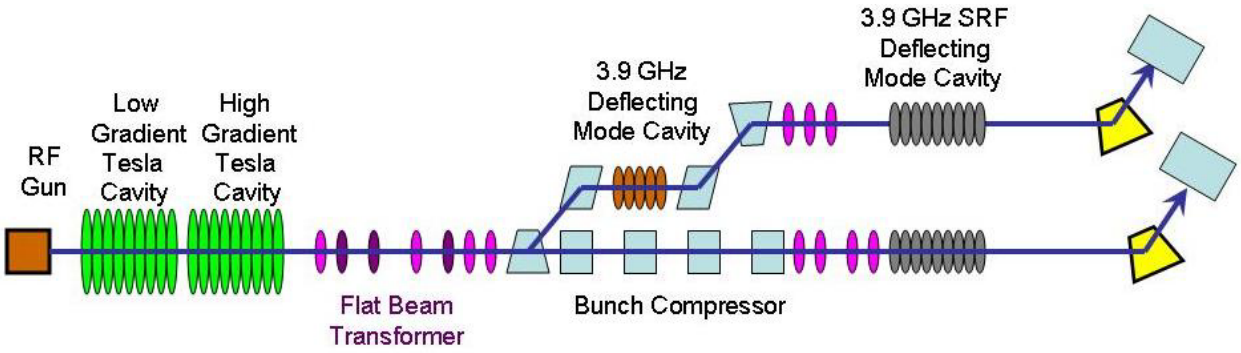

Figure 7.3: A0 upgrade showing 2 accelerating cavities.